Early-life stress and amyloidosis in mice share pathogenic pathways involving synaptic mitochondria and lipid metabolism

Kotah, J.M.; Kater, M.S.J.; Brosens, N.; Lesuis, S.L.; Tandari, R.; Blok, T.M.; Marchetto, L.; Yusaf, E.; Koopmans, F.T.W.; Smit, A.B.; Lucassen, P.J.; Krugers, H.J.; Verheijen, M.H.G.; Korosi, A.

DOI
10.1002/alz.13569

Publication date
2024

Document Version
Final published version

Published in
Alzheimer's & Dementia

Received: 30 May 2023 | Revised: 7 November 2023 | Accepted: 9 November 2023

DOI: 10.1002/alz.13569

Alzheimer's & Dementia®
THE JOURNAL OF THE ALZHEIMER'S ASSOCIATION

RESEARCH ARTICLE

Early-life stress and amyloidosis in mice share pathogenic pathways involving synaptic mitochondria and lipid metabolism

Janssen M. Kotah[1] | Mandy S. J. Kater[2] | Niek Brosens[1] | Sylvie L. Lesuis[1] | Roberta Tandari[1] | Thomas M. Blok[2] | Luca Marchetto[1] | Ella Yusaf[1] | Frank T. W. Koopmans[2] | August B. Smit[2] | Paul J. Lucassen[1] | Harm J. Krugers[1] | Mark H. G. Verheijen[2] | Aniko Korosi[1]

[1]Brain Plasticity Group, Swammerdam Institute for Life Sciences – Center for Neuroscience, University of Amsterdam, Amsterdam, The Netherlands

[2]Department of Molecular and Cellular Neurobiology, Center for Neurogenomics and Cognitive Research, Amsterdam Neuroscience, Vrije Universiteit Amsterdam, Amsterdam, The Netherlands

Correspondence
Dr Aniko Korosi, Brain Plasticity Group, Swammerdam Institute for Life Sciences – Center for Neuroscience, University of Amsterdam, Science Park 904, 1098 XH Amsterdam, The Netherlands.
Email: a.korosi@uva.nl

Janssen M. Kotah and Mandy S. J. Kater shared first authorship.

Mark H. G. Verheijen and Aniko Korosi shared last authorship.

Funding information
Dutch Research Council; Center for Urban Mental Health

Abstract

INTRODUCTION: Early-life stress (ES) increases the risk for Alzheimer's disease (AD). We and others have shown that ES aggravates amyloid-beta (Aβ) pathology and promotes cognitive dysfunction in APP/PS1 mice, but underlying mechanisms remain unclear.

METHODS: We studied how ES affects the hippocampal synaptic proteome in wild-type (WT) and APP/PS1 mice at early and late pathological stages, and validated hits using electron microscopy and immunofluorescence.

RESULTS: The hippocampal synaptosomes of both ES-exposed WT and early-stage APP/PS1 mice showed a relative decrease in actin dynamics-related proteins and a relative increase in mitochondrial proteins. ES had minimal effects on older WT mice, while strongly affecting the synaptic proteome of advanced stage APP/PS1 mice, particularly the expression of astrocytic and mitochondrial proteins.

DISCUSSION: Our data show that ES and amyloidosis share pathogenic pathways involving synaptic mitochondrial dysfunction and lipid metabolism, which may underlie the observed impact of ES on the trajectory of AD.

KEYWORDS
APP/PS1, lipid metabolism, mass spectrometry, mitochondria, synaptosomes

1 | BACKGROUND

Despite advances in our understanding of the role of genetics in Alzheimer's disease (AD),[1,2] recent evidence emphasizes an important additional role of environmental (i.e., non-genetic) factors in its etiology, including, for example, exposure to (chronic) stress.[3–5] Emerging clinical and epidemiological evidence further indicates that in particular a history of early-life stress (ES) might increase the risk to develop later cognitive decline, AD, and other dementias.[6–9]

This association has been further substantiated in studies on transgenic APPswe/PS1de9 (APP/PS1) mice, a popular mouse model of amyloidosis, which overexpress mutated versions of the human amyloid precursor protein and presenilin-1.[10,11] These mutations result in the appearance of amyloid-beta (Aβ) plaques by 6 months of age,[10,11] and are accompanied by altered cognition,[12] synaptic protein expression,[13] and neuroinflammation,[14,15] among other phenotypes. When APP/PS1 mice are exposed to ES, via, for example, the well-established limited bedding and nesting (LBN) model, we and

others have reported age-dependent alterations in plaque load[16] and neuroinflammation,[16,17] as well as deficits in cognitive flexibility,[18] fear learning,[19,20] postsynaptic receptor protein expression,[20] and long term potentiation.[21]

The synapse is a prominently affected substrate in AD patients, who display extensive synaptic loss, especially in their hippocampus.[22,23] This synaptic loss is thought to start early on and to contribute strongly to the cognitive deficits in AD, and many view AD as a synaptic disorder.[24] Synaptic deficits are already present in early and prodromal cases of AD and precede neurodegenerative features of AD.[25] Furthermore, they have been suggested to increase as Aβ pathology accumulates in animal models.[13] However, although synapse (dys)function appears to be a key and early substrate in AD, and ES promotes AD pathology and cognitive deficits, little was known about how ES exposure influences the proteome of the synapse and modulates Aβ-induced synaptic protein alterations.

We therefore set out to study how the synaptic proteome of the hippocampus is affected in APP/PS1 mice during early, pre-plaque stages of pathology, and how these changes compare to more advanced pathological stages. We further assessed how prior ES exposure during the first postnatal week (via the LBN model) modulates these genetically encoded alterations. We studied this using label free mass spectrometry in APP/PS1 mice and their wild-type (WT) littermates at 4 and 10 months of age, representing stages with low and high Aβ pathology, respectively.[16] The hippocampi used in this study were derived from a cohort of APP/PS1 mice from which we had already previously reported the effects of ES on amyloidosis,[16] cognition,[26] neurogenesis,[26] and neuroimmune (i.e., microglial[16] and astrocytic[17]) profiles. Our design studying mice at both ages allowed us to also investigate the trajectory of the identified changes across pathological stages and how this is affected by ES.

At an early pathological stage (4 months), non-stressed APP/PS1 and ES-exposed WT mice presented remarkably similar changes in synaptosomal proteins, which were associated with mitochondria and actin dynamics, and not further altered in ES-exposed APP/PS1 mice. At an advanced pathological stage (10 months), Aβ-associated alterations were pronounced in APP/PS1 brains, with ES-exposure strongly impacting the proteomic profile in APP/PS1 mice, especially proteins related to mitochondrial and lipid metabolism. We validated our main findings via electron microscopy and immunostaining. Lastly, we visualized how ES impacts the trajectory of proteins progressively affected with age by the APP/PS1 genotype, and found that ES-exposure in APP/PS1 mice leads to a distinct trajectory of synaptic protein alterations.

RESEARCH IN CONTEXT

1. **Systematic review**: We reviewed the literature using PubMed. No studies so far examined effects of early-life stress (ES) on the proteomic signature of synapses in wild-type and APP/PS1 mice, across early and advanced pathological amyloid stages.
2. **Interpretation**: At an early pathological stage, the hippocampal synaptosomes of ES exposed wild-type mice and APP/PS1 exhibit similar alterations in proteome signature including alterations in mitochondrial and actin dynamic related proteins. At advanced pathological stage, however, exposure to ES heavily affects the proteome of APP/PS1 mice including astrocytic proteins involved in lipid metabolism. Our study highlights convergent mechanisms underlying ES- and AD pathology-induced synaptic (dys-)function, and thereby provides novel insights into how ES exposure might increase the risk to develop AD.
3. **Future directions**: Future studies should test whether: (1) the ES-induced mitochondrial dysfunction contributes to lipid dyshomeostasis, neuroinflammation, and synaptic dysfunction in AD; and (2) targeting mitochondria may protect against the ES- and AD-induced synaptic and cognitive deficits.

2 | METHODS

2.1 | Animals

For this study, we used male bi-genic hemizygous APPswe/PS1dE9 (TG) mice on a C57Bl/6J background, and their WT littermates.

Mice were bred in-house and kept under standard housing conditions (temperature 20–22°C, 40%–60% humidity level, chow/water ad libitum, 12/12 hour light/dark schedule). All experiments were approved by the Animal Experiment Committees of the Vrije University Amsterdam and the University of Amsterdam.

To investigate how synaptic protein expression is altered by Aβ/PS-1 overexpression, we first compared WT and TG mice sacrificed at 4 months of age (Cohort 1: WT $n = 7$, TG $n = 7$). Next, to test how ES influences the Aβ-induced synaptic protein alterations, we exposed WT and TG mice to control (CTL) or ES conditions during the first postnatal week (for details, see below) and sacrificed them at either an early pathological stage (4 months, Cohort 2: WT-CTL $n = 5$, WT-ES $n = 4$, TG-CTL $n = 4$, TG-ES $n = 4$), or at an advanced pathological stage (10 months, Cohort 3: WT-CTL $n = 5$, WT-ES $n = 9$, TG-CTL $n = 5$, TG-ES $n = 6$).

Two more cohorts were generated to follow up on the proteomics data. Cohort 4 consisted of ES-exposed WT and TG littermates that were sacrificed at 4 months to investigate mitochondria using electron microscopy (WT-CTL: $n = 7$, WT-ES: $n = 5$, TG-CTL: $n = 5$, TG-ES: $n = 6$). Cohort 5 consisted of CTL or ES-exposed TG mice sacrificed at 12 months and was used to validate two proteins that were found to be differentially expressed in the 10 months proteomics data set (TG-CTL: $n = 8$, TG-ES: $n = 6$).

2.2 | Early-life stress paradigm

Mice used in ES experiments were bred and randomly assigned to either control or ES groups at postnatal day (PND) 2 as previously described.[16,17] Briefly, CTL litters were housed in standard amounts of sawdust, along with a 5 × 5 cm piece of paper nesting material (Tecnilab-BMI, Someren, The Netherlands). In contrast, ES nests had half of a 2.5 × 5 cm square of nesting material available and were housed on a fine-gauge stainless steel mesh that was placed above 1/3 of the regular amount of CTL bedding material, that they could not touch. All cages were covered with filter tops. Nests were transferred to standard cage conditions at PND9, and allowed to age, while group-housed with littermates, until used in our experiments.

2.3 | Synaptosome proteomics

2.3.1 | Tissue collection and synaptosome isolation

To study how Aβ pathology affects the hippocampal synaptosome, mice from Cohorts 1, 2, and 3 were sacrificed via rapid decapitation in the morning. The hippocampi of these mice were dissected, snap frozen on dry ice, and stored at −80°C until further use.

Synaptosomes were isolated on a discontinuous sucrose gradient as described previously.[13] In short, homogenization buffer (0.32 M sucrose, 5 mM HEPES, in PBS pH = 7.4, with EDTA-free protease inhibitor cocktail, Roche cOmplete, EDTA-free, 11873580001) was added to hippocampi samples, after which they were mechanically homogenized using a Dounce homogenizer (12 strokes, 900 rpm). Samples were centrifuged at 1000 × *g* for 10 minutes and the supernatant was collected. This supernatant was layered onto a 0.85/1.2 M sucrose gradient and centrifuged at 30,000 × *g* for 2 hours. Synaptosomes were collected from the 0.85/1.2 M interface, diluted with homogenization buffer and centrifuged at 18,000 × *g* for 30 minutes to obtain a synaptosome pellet. The synaptosomes were resuspended in homogenization buffer and stored at −80°C. All steps were performed on ice or at 4°C.

2.3.2 | MS sample preparation

MS sample preparation was performed following the filter-aided sample preparation (FASP) protocol as previously described.[27] For each sample, 10 μg of protein was extracted and reduced in 75 uL of SDS-lysis buffer (2% SDS, 100 mM Tris-HCl pH = 8.8, and 1.33 mM TCEP) at 55°C for 1 hour in a thermomixer set to 900 rpm. Free sulfhydryl groups were alkylated by incubation with 20 mM MMTS for 30 minutes at room temperature (RT). Next, the protein lysate was mixed with 200 uL urea buffer (8 M urea in 100 mM TRIS (pH = 8.8)), cleared of insoluble debris by centrifugation at 20,000 × *g* for 2 minutes at 20°C, and loaded onto a Microcon Ultracel YM-30 filter (Millipore). The filters were centrifuged at 14,000 × *g* for 15 min at 20°C and subsequently washed five times with 200 μL urea buffer and four times with 50 mM NH_4HCO_3 (identical centrifugation settings). Filters were supplemented with 0.6 μg Trypsin/Lys-C (Promega) in 100 μL 50 mM NH_4HCO_3 and incubated overnight at 37°C within a humidified incubator. Digested peptides were eluted from the filters with 50 mM NH_4HCO_3, dried using a SpeedVac and stored at −20°C.

2.3.3 | Micro-LC and SWATH mass spectrometry

Peptides were analyzed by micro-LC MS/MS using an Ultimate 3000 LC system (Dionex, Thermo Scientific, Waltham, MA, USA) coupled to the TripleTOF 5600 mass spectrometer (Sciex, Framingham, MA, USA) as described previously.[13] Peptides were redissolved in 5% acetonitrile (VWR, Radnor, PA, USA) with 0.1% formic acid, trapped on a 5 mm Pepmap 100 C18 column (Dionex, Thermo Scientific, Waltham, MA, USA; 300 μm i.d., 5 μm particle size), and fractionated on a ChromXP C18 column (Eksigent, Sciex, Framingham, MA, USA; 3 μm particle size, 120A). The acetonitrile concentration in the mobile phase was increased from 5% to 18% in 88 minutes, to 25% at 98 minutes, 40% at 108 minutes and to 90% in 2 minutes, at a flow rate of 5 μL/min. The eluted peptides were electro-sprayed into the TripleTOF 5600 mass spectrometer, with a micro-spray needle voltage of 5500 V. SWATH/DIA experiments consisted of a parent ion scan (150 ms, m/z 350–1250) followed by sequential SWATH windows of 8 Da with a scan time of 80 ms, that stepped through the mass range between 450 and 770 m/z with 1 Da overlap. The collision energy for each window was determined based on the appropriate collision energy for a 2+ ion, centered upon the window with a spread of 15 eV.

2.3.4 | SWATH data analysis

Spectronaut version 13.7 (Biognosys, Schlieren, Switzerland) was used to analyze all raw mass spectrometry data. First, an extensive proteomic dataset of fractionated synaptosomal preparations, that were previously measured on the same mass spectrometer in Data Dependent Acquisition (DDA) mode, was imported as a spectral library.[13] Next, Spectronaut was used to search the label-free raw SWATH/DIA data for each (unfractionated) sample in the 4-month dataset for all peptide fingerprints in the spectral library (e.g., expected iRT, charge, mass, fragment intensities) using default settings (at least three fragments per precursor, at least one peptide per protein, 1% FDR for both peptides and proteins). FragmentGroup (MS2) peak areas were used for peptide quantification. The 10-month dataset was processed analogously.

The peptide-centric data report from Spectronaut, which contained confidence scores and abundance values for all peptides identified in the dataset, was further processed using MS-DAP version 0.2.6.3[13] to generate a quality control report and perform statistical analyses. Samples with demonstrable chromatographic aberrations, leading to substantially increased within-group coefficient of variation estimates, were excluded from further analyses. Filtering was performed to retain only peptides that were identified (by Spectronaut) in 75% of replicate

samples in each experimental condition, with at least one peptide per protein required.

Because SWATH/DIA proteomics is known to generate only very few missing values,[28] we expect to perform statistics on the subset of consistently identified peptides and only miss out on proteins that are barely detectable (only observed sporadically) or truly abolished in one experimental condition and not the other when using this filtering approach. The MSqRob algorithm[29] was used to perform differential expression analyses on the peptide abundance values and the resulting protein-level *p*-values were adjusted for multiple testing using the Benjamini-Hochberg procedure.

2.3.5 | Downstream analysis of mass spectrometry data

The threshold for significance was set at FDR < 0.05 (corrected using the Benjamini-Hochberg procedure) and Log2 -fold change cut off at ±0.1. The effect sizes of identified differentially expressed proteins (median Log2 FC of −0.16 to 0.22 across nine contrasts) were comparable to those described in our proteomics studies using the same pipeline.[13,27] Venn diagrams were created using the ggVenndiagram package on R, v1.1.0.[30] To gain insight into whether specific cell-types are more altered based on the differentially expressed proteins, we performed expression-weighted, cell-type enrichment (EWCE) analysis,[31] using a hippocampal single cell RNAseq dataset.[32]

Functional insights in the role(s) of the differentially expressed proteins were obtained by separately analyzing significantly dysregulated up- and down-regulated proteins with gene ontology (GO, based on biological processes [BP], molecular function [MF], and cellular components [CC]) using gProfiler2,[33] as well as SynGO, a curated resource of synaptic proteins that provides BP and CC terms.[34] Because a majority of our significantly dysregulated proteins was not annotated in SynGO, we chose to use gProfiler-based GO as our main downstream analysis, and to analyze our proteins in SynGO only when we obtained neuronal enrichment from EWCE analyses. We focused on BP and CC terms to keep gProfiler- and SynGO-based outputs comparable, although MF terms are also included in the supplementary tables. Overrepresentation analyses were adjusted for multiple testing by the built in methods to calculate the Benjamini-Hochberg FDR in gProfiler2 and SynGO. GO and enrichment analyses were only performed when there were at least five differentially expressed proteins, and GO analyses that yielded > 10 significantly overrepresented terms (FDR < 0.05) were also semantically clustered using RRVGO to reduce redundancy.[35] All GO tables in the figures and supplementary tables include a column "enrichment," based on the recall column output from gProfiler. This represents the percentage of hits from our analyses divided by all genes associated with a certain GO term detected in the background. Lastly, mitochondrial proteins and pathway analyses were done by importing annotations from the MitoCarta3.0 database[36] into gProfiler2. All data visualizations and statistics were performed in RStudio v1.4.1717.[37]

Using these tools, we confirmed the enrichment of bona fide synaptic proteins in our isolated hippocampal synaptosomes. Out of around 3000 proteins identified and used in pairwise relative abundance analysis between experimental groups in each proteomics cohort, at least 674 proteins per contrast mapped to SynGO (Figure S1A), encompassing the spectrum of annotated cellular components and biological processes terms in the database (Figure S1B). We also found an overall overrepresentation of synaptic ontology terms in our identified proteins by performing GO analysis against the "brain background gene-set" used in SynGO (Figure S1C). The enrichment of synaptic proteins was also confirmed by EWCE analysis, where we could demonstrate enrichment of neuron-annotations among our identified proteins (Figure S1D).

2.4 | Ultrastructural analysis of synapses and mitochondria

2.4.1 | Tissue preparation

To further understand what the identified differences in mitochondrial proteins in TG and ES mice at 4 months in the synaptosome fraction mean for mitochondrial structure and general synaptic structure, we subsequently studied these at the ultrastructural level via electron microscopical (EM) analysis. Mice at 4 months (Cohort 4) were sacrificed via transcardial perfusion with ice-cold 4% paraformaldehyde (PFA) in phosphate buffered saline (PBS, pH = 7.4) under anesthesia by 120 mg/kg Euthasol. Whole brains were carefully dissected, not to exert any pressure on the tissue to preserve morphology at EM and were kept in 4% PFA for 24 hours after which the solution was gradually replaced with 30% sucrose in PBS for cryopreservation of the tissue until the brains sank to the bottom of the vial. Brains were stored at −80°C until further processing.

Fifty μm thick coronal sections of the hippocampus were cut on a sliding microtome. For synapse analysis, sections were post-fixed overnight at 4°C using 2.5% glutaraldehyde (Merck-Millipore, 104239) in cacodylate buffer (CB, 0.1 M cacodylate in H_2O, PH 7.4) and, subsequently, washed in CB. Contrasting of the sections was realized using a solution of 1% osmium (Electron Microscopy Sciences, 19172) and 1% ruthenium (Sigma-Aldrich, 378232) in H_2O. The slices were then exposed to increasing ethanol concentrations (30%, 50%, 70%, 90%, 96%, and 100%) and finally propylene oxide for dehydration. Sections were infiltrated with EPON:propylene oxide (1:1) and embedded in EPON. Polymerization was performed for 48–72 hours at 65°C. Ultrathin sections of 90 nm of the dorsal CA1 hippocampus were then cut on an ultra-microtome (Reichert-Jung, Ultracut E). Finally, post-contrast was realized with 1% uranyl acetate and 3% lead citrate in an Ultra-stainer device (Leica EM AC20).

2.4.2 | Electron microscopy imaging and analysis

The grids were examined with a JEOL JEM 1011 electron microscope at 50.000x magnification for mitochondria, and at 100.000x for synapses. Pictures were taken with an Olympus Moreda 11-MP camera and iTEM software (Olympus).

For the analysis of mitochondrial ultrastructure, a total of 70 pictures per animal of randomly selected locations within a section of dorsal CA1 hippocampus (around Bregma point −1.6) were collected in which at least one morphologically intact mitochondrion was identified. Mitochondria within peri-synaptic structures were counted and classified as belonging to either the pre-synapse (based on presence of vesicles), post-synapse (based on presence of postsynaptic densities), dendritic spines (based on elongated form), or astrocytes (based on clear, electron deficient cytoplasm). Morphological features (Perimeter, Area, Circularity) of whole mitochondria (i.e., those not on the edge of the image) were measured using ImageJ. Outliers in the morphological measurements were removed using the 1.5* interquartile range method.

A total of 40 synapses were imaged per animal to quantify synaptic ultrastructural features. Images were blinded using the blind analysis tool in ImageJ and manually quantified. Synaptic vesicles making contact with the active zone were defined as docked. The active zone was identified based on docked synaptic vesicles and a clear density opposing the post synaptic density.

2.4.3 | Statistical analyses

Statistical analyses were done by creating a mixed model to assess the effects of genotype, early-life condition, and their interaction, while correcting for the nesting effect of multiple measures being obtained from the same mice. Post-hoc analyses were conducted correcting using Tukey's method.

2.5 | Immunofluorescence

To validate the ES-induced modulation of at least some elements of the hippocampal synaptic proteome in APP/PS1 mice at advanced stages of pathology, we used two parallel series of 40 μm thick coronal brain slices from a previously described cohort of 12-month-old APP/PS1 mice exposed to ES[19] (Cohort 5). These mice had been sacrificed via rapid decapitation within the first 2 hour of the light phase, and brains were immersion-fixed in 4% paraformaldehyde overnight, then stored in 0.1 M Phosphate Buffer with 0.01% Na-Azide until slicing and stored in antifreeze at −20°C until use.

We immuno-stained against two prominent proteins involved in lipid metabolism, i.e., Hydroxyacyl-CoA Dehydrogenase Trifunctional Multienzyme Complex Subunit Alpha (Hadha, rabbit polyclonal Abcam, ab54477, 1:250) and Fatty Acid Synthase (Fasn, rabbit polyclonal, Abcam ab22759, 1:500). Both were co-stained with Vimentin (chicken polyclonal, EMD Millipore 5733, 1:3000 for Hadha; 1:2000 for Fasn) to co-localize the signals to astrocytes.

Hadha immunostaining was performed on pre-mounted slices after 15 min of antigen retrieval at 100°C in citrate buffer (pH 6.0), whereas Fasn was performed free floating at RT. Both were blocked for 1 hour in a 0.05 M TBS mix with 5% NGS and 0.3% Triton (pH 7.6), then incubated with primary antibodies for 1 hour at RT, then overnight at 4°C. Sections were incubated the next day with secondary antibodies (goat anti-chicken-A488, goat-anti-rabbit-A568, and goat-anti-mouse-A647, Invitrogen, 1:800) for 2 hours at RT. Slices were washed with 0.05 M TBS (pH 7.6) between steps. We used 12 brains (TG-CTL: $n = 7$, TG-ES: $n = 5$) for Hadha staining and 14 brains (TG-CTL: $n = 8$, TG-ES: $n = 6$) for Fasn staining.

2.6 | Confocal microscopy and image analysis

We imaged 1 μm-step Z-stacks (total Z range of 9 to 10 μm) at 40x magnification using a Nikon A1 confocal microscope. Images were taken from six sections collected at an equidistant sampling along the dorsoventral axis of the hippocampus to obtain an adequate representation of the structure. Each image was digitally stitched into one composite image such that all hippocampal subregions (stratrum oriens in the cornu ammonis [CA] to the hilus in the dentate gyrus [DG]) were visible, with dorsal sections being two images wide and four images tall and ventral sections being four or five images wide and three images tall.

Images were analyzed with FIJI (v1.53q) by first drawing regions of interest to define the CA and DG regions. Total coverage was calculated by dividing the total Hadha/Fasn automated thresholded signal by the surface area of the regions of interest. To measure astrocytic expression of Hadha/Fasn, images were preprocessed by generating binary masks of Vimentin signal using an automated threshold followed by particle analysis at each image on the z-stack. Hadha and Fasn signals outside the Vimentin masks were cleared, and the remaining automated thresholded signal was divided by the area of the Vimentin masks to calculate their astrocytic coverage. After testing for outliers using the 1.5*interquartile range method, data were analyzed using the student's t-test.

2.7 | Visualizing trajectories of proteomic alterations from 4 to 10 months

To visualize the trajectory of transgenic APP/PS1 (TG-) induced effects at the synapse, and possible further modulations by ES exposure, we adopted a descriptive ΔLog2FC approach to visualize temporal dynamics of changes in synaptosomal proteomes.[13] We first selected proteins of interest based on their differential expression between 4 and 10 months in our contrasts of interest ("WT-CTL vs. TG-CTL" and "TG-CTL vs. TG-ES"). Then, for each protein, we calculated a ratio between the Log2FC across ages ($Log2FC_{10months}/Log2FC_{4months,}$ or ΔLog2FC) in each contrast. Subsequently, we arranged differentially expressed

proteins in order of their ΔLog2FC values, noting the congruence between these values across both contrasts. We also highlighted within this list the proteins involved in mitochondrial,[36] cytoskeletal (GO:0005856 from AmiGO2 v2.5.17[38]), and synapse-specific astrocytic[39] function, based on literature-defined gene sets.

3 | RESULTS

3.1 | Early Aβ pathology alters hippocampal synaptic proteins involved in mitochondria and actin dynamics

To identify possible synaptic alterations induced by the transgenic APP/PS1 genotype (TG) at early stages of Aβ pathology, we characterized the proteome in hippocampal synaptosomes from WT and TG mice at 4 months of age (4 months; Cohort 1, Figure 1A). Because the cohort generated to investigate early-life stress (ES) effects on TG mice also included WT and TG groups that were not exposed to ES (Cohort 2, Figure 1B), we present them here together. We found a similar number of differentially expressed proteins (relative to WT) in both cohorts (Cohort 1: 14 up, 23 down; Cohort 2: 17 up, 23 down, Figure 1C-E, Table S1, S2), of which two proteins (Abi1, Wasf) were consistently relatively downregulated in both cohorts.

Overrepresented GO terms, based on differentially expressed proteins in both cohorts, were related to the same processes, i.e., mitochondria and actin dynamics (Figure 1F, 1G, Table S3), but notably involved different sets of proteins. Both cohorts displayed an overrepresentation of terms related to the mitochondrial membrane (Timm50, Them4, Pnpla8, Acsl6, Aldh3a2, Sdhd, Sfxn5) in relatively upregulated proteins, which were also overrepresented for fatty acid and monocarboxylic acid metabolism (Acsl6, Aldh3a2, App, Echs1, Pnpla8, Them4) in Cohort 1.

This mitochondrial alteration was also evident when comparing the relatively upregulated proteins with a curated database of mitochondrial proteins (MitoCarta3.0[36]), with nine such proteins in Cohort 1 (Acsl6, Aldh3a2, Echs1, Nipsnap3b, Pnpla8, Sdhd, Sfxn5, Them4, Timm50) and seven in Cohort 2 (Bcs1l, Coa3, Eci1, Htra2, Lactb, Ndufa7, Prkaca).

We also found in both cohorts a relative downregulation of proteins (*Cohort 1*: Abi1, Cyfip2, Wasf1; *Cohort 2*: Abi1, Nckap1, Wasf) involved in the SCAR complex, which plays a role in actin dynamics and cytoskeletal regulation,[40] which notably included the two shared downregulated proteins (Abi1, Wasf). The relative downregulation of actin-related proteins in synaptosomes from TG mice was particularly evident in Cohort 2 (Figure 1F), wherein actin-related biological processes (e.g., polymerization/depolymerization: Abi1, Add2, Capza1, Capza2, Capzb, Dbn1, Nckap1, Pfn1, Pfn2, Ppp1r9b, Tmod2) were overrepresented. In terms of cellular component annotations, these proteins were annotated to the cytoskeleton and the post-synapse (Figure 1G, Table S3).

To assess whether the list of relatively up- and downregulated proteins in both cohorts reflected cell-type specific TG effects, we performed expression-weighted cell-type enrichment (EWCE) analysis[31] using a published single-cell gene expression database from the mouse hippocampus.[32] TG synaptosomes from Cohort 1 exhibited astrocytic enrichment in the relatively upregulated proteins and a neuronal enrichment in the relatively downregulated proteins (Figure S2A). In Cohort 2, we did not detect any cell type enrichment in relatively upregulated proteins, while the relatively downregulated proteins were enriched for neurons (Figure S2B). Because of the neuronal annotation of the relatively downregulated proteins in both cohorts, we then further characterized their function using SynGO, and found these to be involved in postsynaptic processes, specifically with respect to actin-related processes (Figure S2C-D, Table S4).

3.2 | ES downregulates actin dynamics and upregulates astrocytic proteins in hippocampal synaptosomes from WT mice at 4 months

We next investigated how ES exposure affected the synaptic proteome in 4-month-old WT and TG mice (Figure 2A). ES exposure in WT animals resulted in 126 differentially expressed synaptosomal proteins (84 up, 42 down, Figure 2B, Table S2). Based on GO analyses, a protein group relatively enriched in WT-ES synaptosomes contained, for example, Atp1a2, Atp1b2, Gnai2, Slc1a3, Slc8a1, i.e., ATPase subunits as well as Glutamate and GABA transporters, and were associated with cellular component terms such as the GTPase complex, and endoplasmic reticulum of the cell (Figure S2E, Table S3). We also found evidence for mitochondrial involvement in these proteins, with an overrepresentation of mitochondria-associated membrane of the endoplasmic reticulum (Bcap31, Canx, Tmx2, Table S3). The 126 relatively upregulated proteins were revealed by EWCE analysis to have enriched astrocytic annotations (Figure 2C). In line with this, some of these upregulated proteins have been described in literature to be specific for astrocytic proteins enriched around the synapse, for example, Atp1a2,[41] Slc1a2,[41] Slc1a3,[41] and Slc6a11.[42] GO analysis of relatively downregulated proteins revealed an overrepresentation of biological process terms, such as actin cytoskeletal dynamics (via Abi2, Actn4, Add2, Bin1, Capza1, Capza2, Capzb, Cfl1, Coro1c, Dbn1, Pfn2, Ppm1e, Ppp1r9b, Tmod2, Twf2), and cellular component terms, such as axonal growth cones (via Cfl1, Dbn1, Fkbp4, Hsp90ab1, Ppp1r9b, Tmod2, Twf2, Figure S2F, Table S3).

3.3 | Similar effects of ES exposure and APP/PS1 genotype on the hippocampal synaptic proteome at 4 months

ES exposure did not lead to significant changes in synaptosomal protein expression within TG mice at this age (Table S2). This is in contrast to found alterations in synaptosomes when comparing either TG-CTL or WT-ES mice to WT-CTL mice, suggesting a degree of convergence between ES and TG effects at this age. To explore this, we investigated

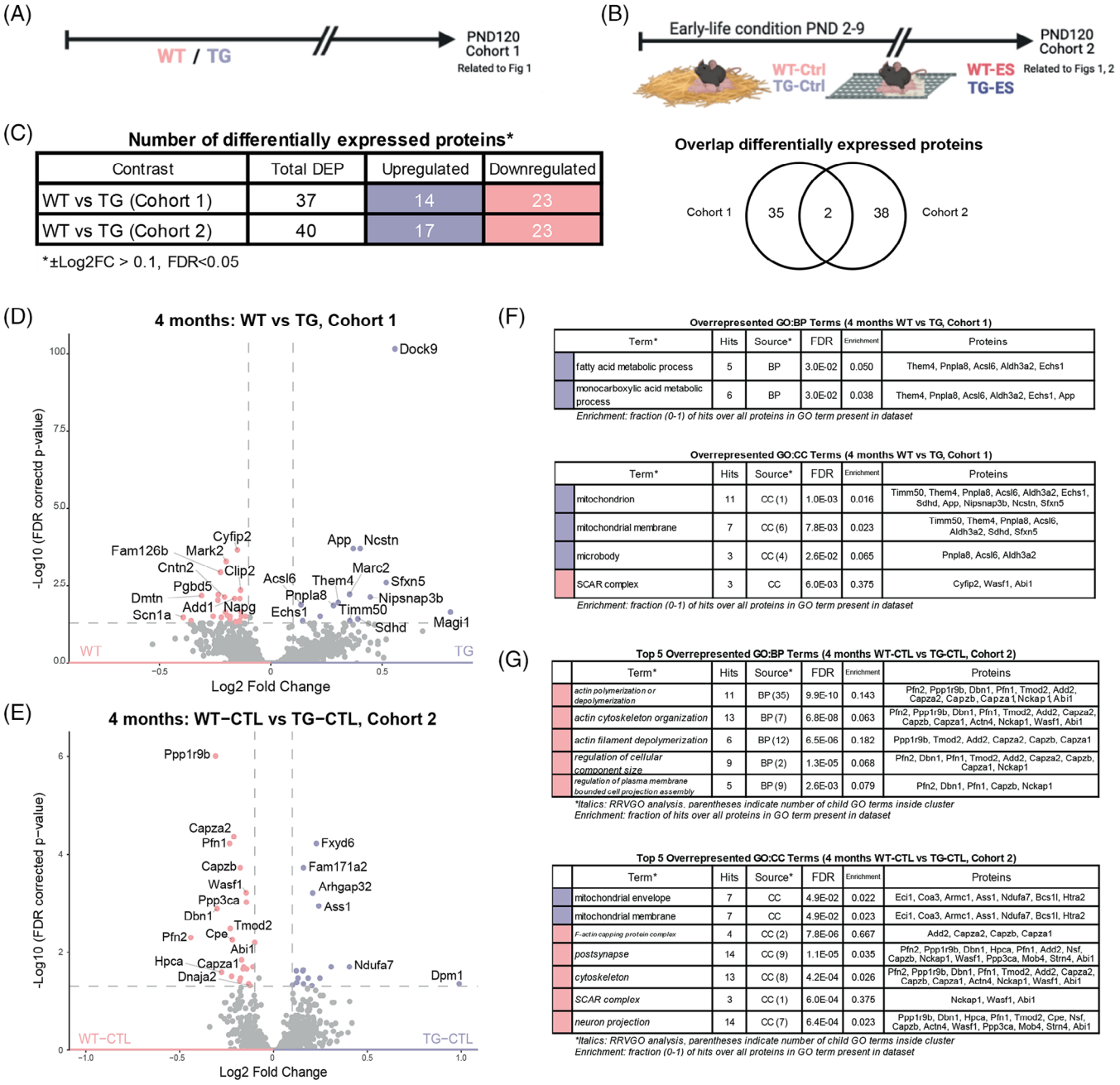

FIGURE 1 Synaptosomal upregulation of mitochondrial proteins and downregulation of actin-dynamics proteins in 4 months APP/PS1 mice. (A,B) Experimental design in analyzing the hippocampal synaptosomal proteome at four months of age (4 months) in Cohorts 1 (A) and 2 (B). Created with Biorender.com. (C) Table summarizing differentially expressed proteins between two cohorts of wild-type (WT) and transgenic APP/PS1 (TG) mice. Only two proteins (Abi1, Wasf) were significantly downregulated in both cohorts. (D,E) Volcano plots showing differentially expressed proteins (± Log2FC > 0.1, FDR < 0.05) in cohorts 1 (D) and 2 (E). (F,G) Overview of overrepresented biological processes (BP) and cellular component (CC) terms based on gene ontology (GO) analyses of up- (light blue) and downregulated (light red) proteins in Cohorts 1 (F) and 2 (G). Italicized terms are "parent" GO terms after clustering by semantic similarity using RRVGO. Volcano plots show log-fold change (Log2FC) on the x-axis, and -log10 transformed *p*-values from the MSqRob statistical model, adjusted for multiple testing using the Benjamini-Hochberg procedure on the y-axis.

the 18 proteins (7 up, 11 down) that were differentially expressed in the synaptosomes of both TG-CTL or WT-ES mice (Figure 2D, Table S5). While the group of relatively upregulated proteins did not show any overrepresentation of GO terms, the relatively downregulated proteins were associated with actin-related biological processes (e.g., actin polymerization or depolymerization: Add2, Capza1, Capza2, Capzb, Dbn1, Pfn2, Ppp1r9b, Tmod2) and were overrepresented for cellular component terms, such as the postsynapse (Add2, Capzb, Dbn1, Mob4, Nsf, Pfn2, Ppp1r9b) and dendritic spines (Capzb, Dbn1, Mob4, Ppp1r9b, Table S5).

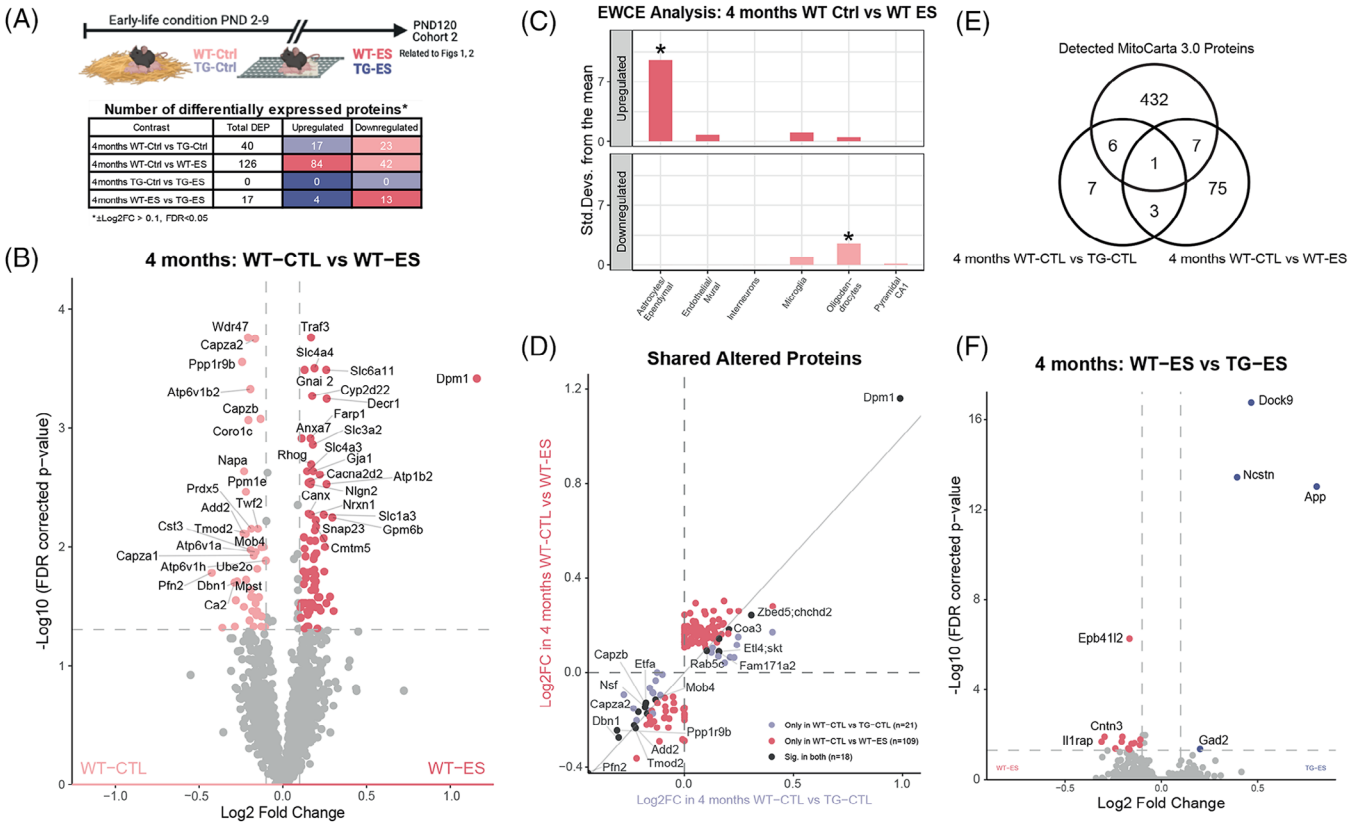

FIGURE 2 Early-life stress (ES) exposure upregulates astrocytic mitochondrial proteins and downregulates actin-dynamics related proteins. (A) Experimental design within cohort 2, consisting of wild-type (WT) and transgenic APP/PS1 (TG) mice exposed to control (CTL) or early-life stress (ES) at 4 months of age (4 months), and a summary of differentially expressed proteins across contrasts. Created with Biorender.com. (B) Volcano plot showing differentially expressed proteins (± Log2FC > 0.1, FDR < 0.05) in synapses from ES-exposed WT mice. (C) Expression weighted cell type enrichment (EWCE) analysis shows enrichment of astrocytic annotations in upregulated proteins and oligodendrocytic annotations in downregulated proteins. (D) Overlap of differentially expressed proteins when comparing proteomic changes in synaptosomes from TG (light blue) and ES (dark red) mice. (E) Upregulated proteins in synaptosomes from TG-CTL and WT-ES mice are mitochondrial, as determined by the MitoCarta database. (F) Volcano plot showing differentially expressed proteins (± Log2FC > 0.1, FDR < 0.05) when comparing synapses from ES-exposed WT and TG mice. Volcano plots show log-fold change (Log2FC) on the x-axis, and -log10 transformed *p*-values from the MSqRob statistical model, adjusted for multiple testing using the Benjamini-Hochberg procedure on the y-axis.

Beyond shared alterations to actin-related processes, inspection of the shared upregulated proteins also suggested mitochondrial changes in both ES and TG synaptosomes. This is evidenced firstly by the reported mitochondrial expression of Dpm1,[43] the protein with the highest log2-fold change value in TG-CTL (Figure 1D) and WT-ES (Figure 2B) synaptosomes. Several shared, relatively upregulated proteins are also either expressed in mitochondria (e.g., Coa3,[44] Chchd2[45]), or have been reported to interact with mitochondria and to regulate their function (e.g., Rab5c,[46] Etl4-Skt,[47] Slc4a3[48]). Last, several relatively upregulated proteins in synaptosomes isolated from WT-ES mice also overlapped with MitoCarta (Acaa2, Acad8, Acadm, Coa3, Decr1, Glud1, Idh2, Etfa, Mpst, Ndufa3, Prdx5, Figure 2E), similar to the proteins identified when comparing TG-CTL versus WT-CTL synaptosomes.

Next to the overlap between ES and TG effects on synaptosomal protein expression, comparison of ES-exposed WT and TG mice revealed an additional 17 proteins as a result of Aβ overexpression (4 up, 13 down, Figure 2F, Table S2). Relatively upregulated proteins here are involved in Aβ processing (App, Dock9, Ncstn) and GABA biosynthesis (Gad2), while SynGO and GO:CC analyses revealed relatively downregulated proteins to associate with postsynaptic membrane receptor levels (Ctnnd2, Agap3, Snap23, Figure S2G, Table S4) and the hippocampal CA3 mossy fiber synapse (Adcy1, Shank2, Syt7, Table S3), respectively.

3.4 | Ultrastructural analyses at 4 months reveal a loss of mitochondrial numbers in synapses in the hippocampus of both APP/PS1 and ES-exposed mice

Based on the recurrence of mitochondrial terms in our proteomics data, we hypothesized that this organelle might be a convergent substrate through which Aβ overexpression, ES-exposure, or both, alter the hippocampal synapse. We explored this in a follow-up cohort of 4 months WT and TG mice exposed to ES in order to study their mitochondria at the ultrastructural level (Figure 3A, Table S6).

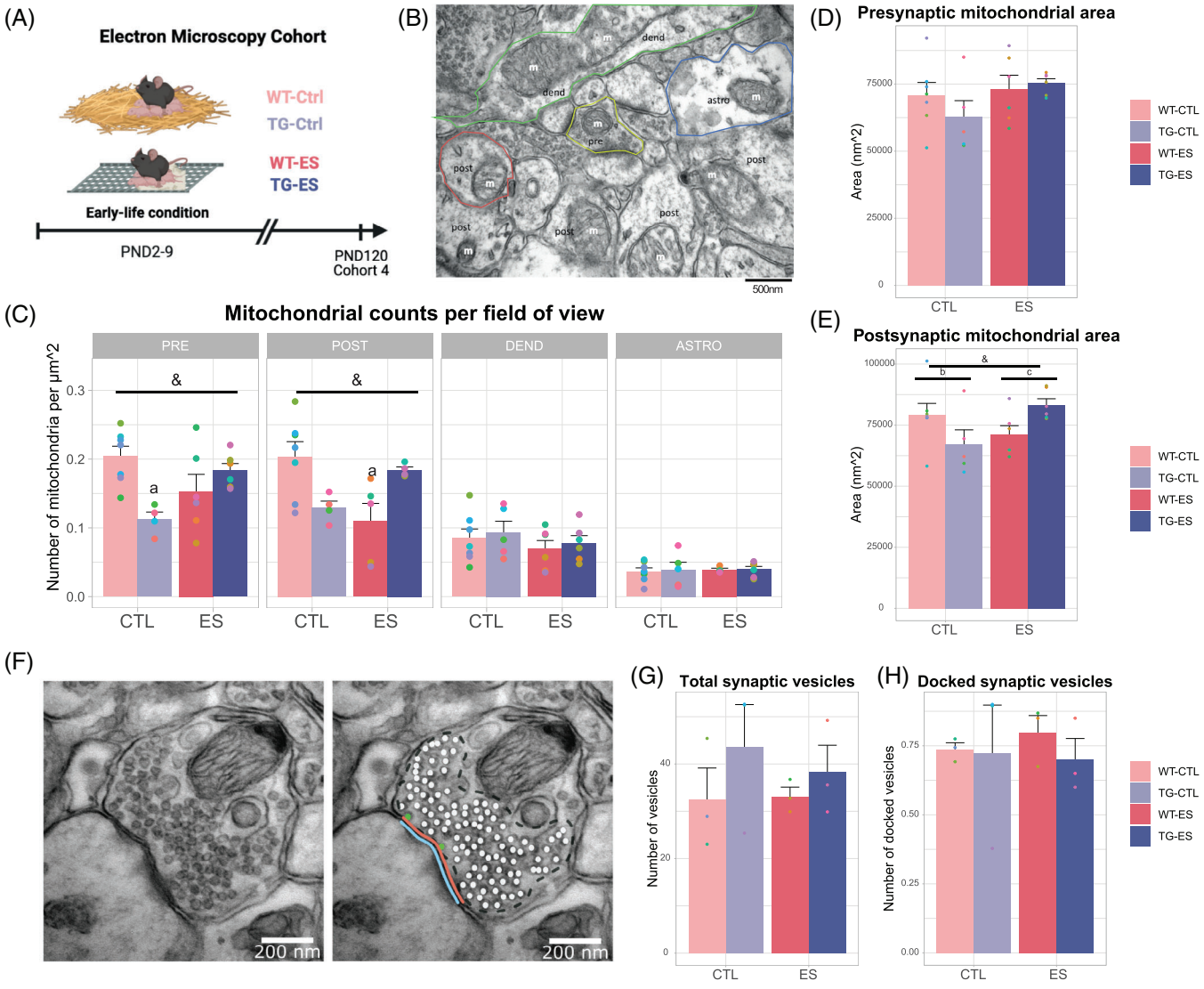

FIGURE 3 Investigating ultrastructural alterations to synaptic mitochondria in ES-exposed WT and TG mice. (A) Overview of cohort 4, consisting of wild-type (WT) and transgenic APP/PS1 (TG) mice exposed to control (CTL) or early-life stress (ES) at 4 months of age (4 months), which was generated for electron microscopy (EM) analysis of mitochondria. Created with Biorender.com. (B) Representative EM image analyzed for mitochondrial analyses. Mitochondria (m) at the CA1 region of the hippocampus were counted and traced across 70 images per animal to analyze their morphology. Analysis was done separately in sub-synaptic structures, as labeled and outlined in the image: presynapse (yellow), postsynapse (red), astrocyte (blue), dendritic compartment (green). (C) Interaction of TG and ES effects on mitochondrial counts at the pre- and post-synapse, but not in dendrites or astrocytes. (D) Alterations to presynaptic mitochondrial counts are not accompanied by alterations to mitochondrial size. (E) Interaction of TG and ES effects on mitochondrial area at the postsynapse. &, interaction effect, $p < 0.05$; post-hoc effects: a, different from WT-CTL, $p < 0.05$; b, difference between WT-CTL and TG-CTL, $p < 0.05$; c, difference between WT-ES and TG-ES, $p < 0.05$. (F) Representative EM image of an analyzed synapse (left) with an example of the different measurements (right): synaptic vesicles (white), docked synaptic vesicles (green), active zone (red), post synaptic density (blue), and synaptic vesicle cluster (dashed line). (G,H) Quantified ultrastructural features of synapses were not affected in APP/PS1 or ES mice, including the total number of synaptic vesicles (G) and the number of docked synaptic vesicles (H). Mitochondrial analyses performed using a mixed linear model, WT-CTL: $n = 7$, WT-ES: $n = 5$, TG-CTL: $n = 5$, TG-ES: $n = 6$. Synapse analyses performed using a mixed linear model, WT-CTL: $n = 3$, WT-ES: $n = 3$, TG-CTL: $n = 3$, TG-ES: $n = 3$.

We determined the number of mitochondria and assessed mitochondrial morphology at the ultrastructural level within the pre-synapse, post-synapse, dendrites, and astrocytes in the CA1 subregion of the hippocampus of these mice (Figure 3B).

While there was no overall TG or ES effect on total number of mitochondria (Figure S3A), we found interaction effects of both factors on the number of mitochondria in the pre-synapse (condition: $F(1,19) = 0.0218$, $p = 0.8842$; genotype: $F(1,19) = 2.1204$, $p = 0.1617$; interaction: $F(1,19) = 12.001$, $p = 0.0026$) and post-synapse (condition: $F(1,16) = 2.5384$, $p = 0.1307$; genotype: $F(1,16) = 0.0555$, $p = 0.8168$; interaction: $F(1,16) = 11.8658$, $p = 0.0033$, Figure 3C). Mitochondria within astrocytes or dendritic structures were not affected. Using pairwise post-hoc tests, we found the pre-synaptic effect to be due to a decrease in mitochondria in TG-CTL compared to WT-CTL synapses

($p = 0.0109$), whereas the postsynaptic interaction effect was driven by a decrease in the number of mitochondria in WT-ES compared to WT-CTL synapses ($p = 0.0171$).

The effects on mitochondrial numbers were not accompanied by alterations in mitochondrial surface area at the pre-synapse (Figure 3D), although there was an interaction between TG and ES effects on the postsynaptic mitochondrial area (Figure 3E, condition: $t(20) = -1.7961$, $p = 0.0876$; genotype: $t(20) = -2.2274$, $p = 0.0376$; interaction: $t(20) = 3.3099$, $p = 0.0035$). Post-hoc analyses reveal that this interaction is explained by significant but opposite effects of genotype in CTL ($t(20) = 2.227$, $p = 0.0376$) and ES ($t(20) = -2.452$, $p = 0.0235$) synapses. Mitochondrial area in dendrites and astrocytes, as well as perimeter and circularity in all measured mitochondria, were not significantly altered by either experimental variable (Figure S3B-D).

Next, we determined whether the observed changes in mitochondrial counts and surface area are accompanied by ultrastructural changes in synapses, as reported in post-mortem human AD brains.[49] We found no changes in synaptic vesicle count (Figure 3G), the number of docked vesicles (Figure 3H), active zone length (Figure S3E), post synaptic density length (Figure S3F), synaptic vesicle cluster size (Figure S3G), synaptic vesicle density (Figure S3H), or the density of docked synaptic vesicles at the active zone (Figure S3I) in any of our experimental groups. This indicates that the observed mitochondrial changes at this age are not accompanied by other ultrastructural synaptic changes.

3.5 | At 10 months of age, APP/PS1 synaptosomes exhibit relative downregulation of proteins involved in presynaptic vesicle release and postsynaptic receptor endocytosis

We further characterized the effects of TG genotype and prior ES exposure on the hippocampal synaptosomal proteome in 10-month-old (10 months) mice (Figure 4A). Synaptosomes isolated from TG-CTL mice showed large relative abundance differences at this age, resulting in 170 dysregulated proteins (11 up, 159 down, Figure 4B, Table S7), which were largely distinct from differentially expressed proteins in TG-CTL synaptosomes at 4 months (Figure 4C). Relatively upregulated proteins in 10 months TG-CTL mice were overrepresented for 52 clusters of biological processes and 13 clusters of cellular components GO terms, mostly driven by App-associated pathways and Aβ-associated neuroinflammation due to differential expression of App, Apoe, and Clu (Table S7). Relatively downregulated proteins were significantly associated with 23 clusters of BP and 17 clusters of CC, including cell communication, neuronal projection development, transport vesicle membranes, and DNA damage (Figure S4A-B, Table S8).

Cell type enrichment analysis using EWCE revealed relatively upregulated proteins to be microglial and astrocytic, whereas relatively downregulated proteins were mostly neuronal (Figure 4D), consistent with the well-documented neuroinflammatory activation[50] and synaptic dysfunction[24] that results from Aβ pathology. To further investigate the synaptic pathways associated with the relatively downregulated proteins, we performed an overrepresentation analysis for biological processes using SynGO (Figure 4E, S4C, Table S4). This analysis revealed an under-representation of proteins in the synapses of 10 months TG mice involved in both presynaptic vesicle exocytosis (via Git1, Ppfia3, Rab3a, Rimbp2, Rph3a, Stx1a, Stxbp1, Sv2b, Syp, Syt7, Vamp2), as well as postsynaptic organization (via Actb, Dlg1, Dlg3, Git1, Mpp2, Rimbp2) and receptor endocytosis (via Akap5, Ap2b1, Ap2m1, Ap2s1, Hpca, Synj1).

The effects of amyloidosis on synaptosomal proteins were also evident when comparing ES-exposed WT and TG mice (Figure 4F), in which 44 proteins were differentially expressed (35 up, 9 down, Table S7). Upregulated proteins were similarly associated with known Aβ-processing pathways, including annotations to cellular components such as high-density lipoproteins, lysosomes, and mitochondria (Table S8). Checking SynGO annotations on the nine relatively downregulated proteins revealed alterations to both pre-and post-synaptic compartments, with no further significant sub-terms (Figure S4D). Notably, 11 out of 44 differentially expressed proteins (upregulated: ApoE, App, Clu, Dock9, Gfap, Nctsn; downregulated: Lgi1, L1cam, Mpp3, Slc30a3, Syt7) were similarly differentially expressed between synaptosomes from TG-CTL and WT-CTL mice, suggesting these to be 'core' alterations that Aβ pathology induces on hippocampal synaptosomes at this age.

3.6 | Prior ES exposure strongly alters the proteome of hippocampal synaptosomes from APP/PS1, but not WT mice, at 10 months of age

We previously hypothesized that ES-associated effects at later ages would be minimal at baseline, but would be more pronounced upon exposure to subsequent challenges later in life.[51] In line with this, and in contrast to the data at 4 months, only 19 proteins (13 up, 6 down) were differentially expressed in 10 months ES-exposed WT synapses (Figure 5A, Table S7). Relatively upregulated proteins did not fit into canonically brain-related pathways, with one overrepresented biological process involving blood pressure regulation (Figure S4E-F). Relatively downregulated proteins were associated with 19 clusters of GO terms (13BP, 6 CC) involving endoplasmic reticulum calcium transport (Figure S4 E-F, ATP2A2, RYR2, Table S8). Also, in contrast to the data at 4 months, where we found 18 shared differentially expressed proteins between ES and TG effects, only one protein (KCNQ2) was significantly altered in both contrasts at 10 months.

Furthermore, while ES did not have lasting effects on synaptosomes from WT mice, we found that ES-exposure massively shifted the proteomic profile of synaptosomes from TG mice at 10 months, with 561 differentially expressed proteins (549 up, 12 down, Figure 5B, Table S7). GO analysis of the relatively upregulated proteins (Figure S4G-H, Table S8) revealed terms related to the metabolism of different molecules such as carbohydrates, aldehydes, NAD, organonitrogens, organophosphates, hydroxy-compounds, as well as GO terms related to DNA metabolic processes and chromosome structure. Cellular

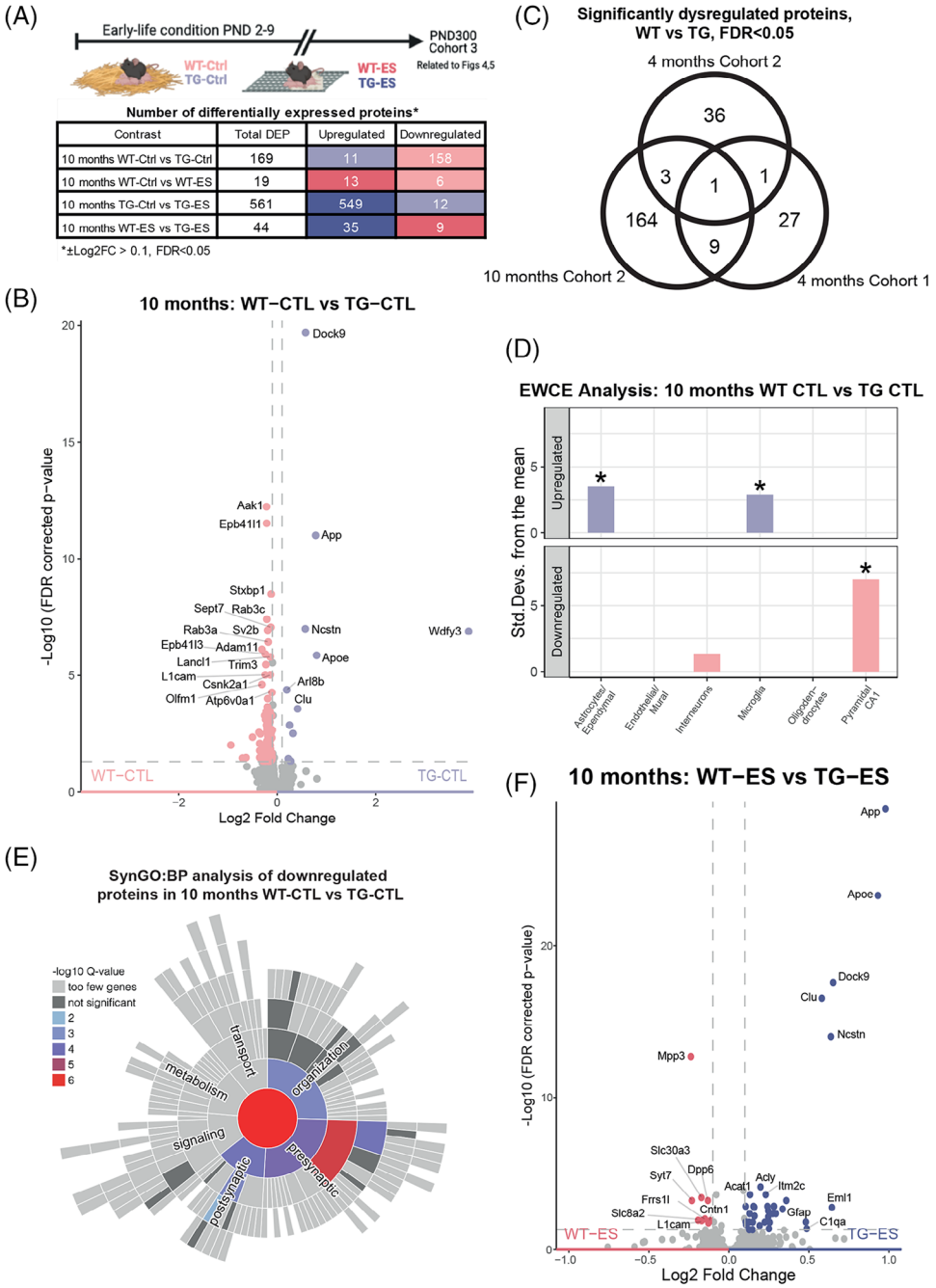

FIGURE 4 Downregulation of proteins involved synaptic transmission in hippocampal synaptosomes from APP/PS1 mice at 10 months (A) Experimental design within cohort 3, consisting of wild-type (WT) and transgenic APP/PS1 (TG) mice exposed to control (CTL) or early-life stress (ES) at 10 months of age (10 months), and a summary of differentially expressed proteins across contrasts. Created with Biorender.com. (B) Volcano plot showing differentially expressed proteins (± Log2FC > 0.1, FDR < 0.05) in synaptosomes from TG-CTL mice at 10 months. (C) Protein alterations in synaptosomes from 10 months TG mice are distinct from changes in TG mice at 4 months. (D) Expression weighted cell type enrichment (EWCE) analysis shows enrichment of astrocytic and microglial annotations in upregulated proteins in synaptosomes from TG-CTL mice. Downregulated proteins are enriched for annotations of excitatory neurons. (E) Further analysis of overrepresented biological processes in downregulated proteins using SynGO (SynGO:BP) reveal disruptions to synapse organization, presynaptic function, and postsynaptic processes. (F) Volcano plot showing differentially expressed proteins (± Log2FC > 0.1, FDR < 0.05) between in ES-exposed WT and TG mice at 10 months. Volcano plots show log-fold change (Log2FC) on the x-axis, and -log10 transformed *p*-values from the MSqRob statistical model, adjusted for multiple testing using the Benjamini-Hochberg procedure on the y-axis.

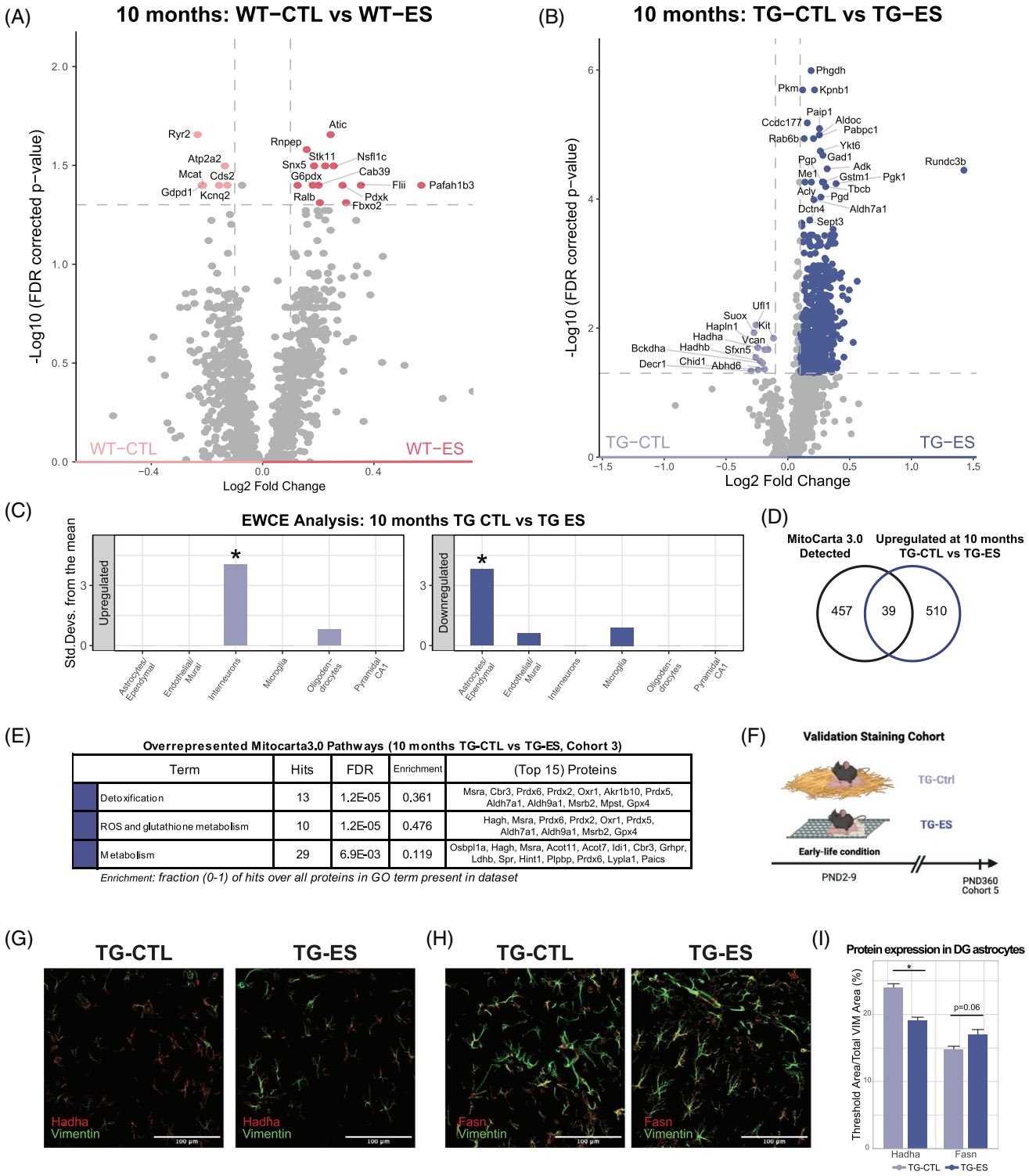

Term	Hits	FDR	Enrichment	(Top 15) Proteins
Detoxification	13	1.2E-05	0.361	Msra, Cbr3, Prdx6, Prdx2, Oxr1, Akr1b10, Prdx5, Aldh7a1, Aldh9a1, Msrb2, Mpst, Gpx4
ROS and glutathione metabolism	10	1.2E-05	0.476	Hagh, Msra, Prdx6, Prdx2, Oxr1, Prdx5, Aldh7a1, Aldh9a1, Msrb2, Gpx4
Metabolism	29	6.9E-03	0.119	Osbpl1a, Hagh, Msra, Acot11, Acot7, Idi1, Cbr3, Grhpr, Ldhb, Spr, Hint1, Plpbp, Prdx6, Lypla1, Paics

Enrichment: fraction (0-1) of hits over all proteins in GO term present in dataset

FIGURE 5 ES exposure further alters (astrocytic) mitochondrial lipid metabolism in TG synaptosomes with advanced pathology. (A) Volcano plot showing differentially expressed proteins (± Log2FC > 0.1, FDR < 0.05) in ES-exposed WT at 10 months. (B) Volcano plot showing further differential expression in synapses from ES-exposed TG mice at this age. (C) Expression weighted cell type enrichment (EWCE) analysis shows enrichment for interneuronal annotations in upregulated proteins in ES-exposed TG mice. Downregulated proteins are enriched for astrocytic annotations. (D,E) Differentially expressed proteins in this contrast overlap with MitoCarta (D) and are functionally annotated to detoxification and reactive oxygen species metabolism (E). (F-I) Overview of cohort 5 (F, created with Biorender.com), used to confirm lasting alterations to astrocytic expression of Hadha (G) and Fasn (H) within ES-exposed TG hippocampus at 12 months (I). Representative images show Vimentin signal in green and filtered Hadha/Fasn signal within Vimentin masks in red. *, condition effect, $p < 0.05$. Analyses performed using student's T test, Hadha – TG-CTL: $n = 7$ TG-ES: $n = 5$, Fasn – TG-CTL: $n = 8$ TG-ES: $n = 6$. Volcano plots show log-fold change (Log2FC) on the x-axis, and -log10 transformed p-values from the MSqRob statistical model, adjusted for multiple testing using the Benjamini-Hochberg procedure on the y-axis.

component analysis indicated 8 clusters of GO terms that suggest alterations at the nucleus, cytosol, (microtubule) cytoskeleton, proteasome complex, and V-type proton ATPases. GO terms that were associated with relatively downregulated proteins in CTL versus ES TG mice (Figure S4G-H, Table S8), were involved in fatty acid metabolism and beta-oxidation in the mitochondria, driven by four proteins (Bckdha, Decr1, Hadha, Hadhb).

EWCE analysis of the differentially expressed proteins revealed the relatively upregulated proteins to be related to interneurons and relatively downregulated proteins to be astrocytic (Figure 5C). Relatively upregulated proteins were not enriched for any SynGO annotated pathways (not shown). Additionally, ES exposure strongly affected mitochondrial proteins in TG synaptosomes at this age, with 47 out of 565 differentially expressed proteins (41 up, 6 down) overlapping with MitoCarta (Figure 5D, in contrast with two mitochondrial proteins, HMCL and MPST, altered between WT-CTL and TG-CTL synaptosomes). GO analysis on these 47 proteins using MitoCarta-annotated pathways revealed an overrepresentation of proteins associated with type II fatty acid synthesis, detoxification, ROS/glutathione metabolism, and sulfur metabolism (Figure 5E). In conjunction with the gene ontology results, these data suggest mitochondrial alterations to underlie the effects of ES exposure on the synaptosomes of TG mice.

To validate the results from the proteomic analysis, and also investigate the temporal persistence of the presumed ES effects on lipid metabolism in the hippocampi of TG mice, we stained against Hadha and Fasn (down- and upregulated in the proteomics data, respectively) in a cohort of 12-month-old TG mice exposed to ES (Cohort 5, Figure 5F, Table S6). Because of the strong expression of these two proteins in astrocytes,[52,53] and as the EWCE data suggested further astrocytic dysfunction in ES-exposed TG mice, we quantified the expression of these proteins together with Vimentin as an astrocyte-specific marker (Figure 5G, 5H). We found a decrease in astrocytic Hadha ($t(9.98) = 2.2486$, $p = 0.0483$, Figure 5I) and a trend for increases in astrocytic Fasn ($t(6.422) = -2.2454$, $p = 0.0630$, Figure 5I), specifically within the entire DG of the hippocampus. The total coverage of Hadha and Fasn immunoreactive signal (i.e., including signals outside astrocytes, Figure S5A-B), as well as of the total Vimentin coverage (Figure S5C), was not different in the whole DG of ES-exposed TG mice. Whether differences between different DG compartments and between astrocyte subtypes within the DG exist, as recently reported,[54,55] awaits further study. None of these measures was significantly altered between groups in the CA regions (Figure S5D-F). These results suggest that the observed alterations to hippocampal lipid metabolism in ES-exposed TG mice might be specific to astrocytes.

3.7 | ES modulates the temporal pattern of synaptic mitochondrial protein alterations seen in TG mice

Last, we contextualized the alterations caused by ES exposure in TG mice, by visualizing the overall change in expression of amyloidosis- and early-life-stress-associated proteins over time. We first selected for proteins that were differentially expressed ($\pm$ Log2FC > 0.1, FDR < 0.05) in either "WT-CTL versus TG-CTL" or "TG-CTL versus TG-ES" contrasts at either 4 or 10 months (Figure 6A). This resulted in 201 differentially expressed proteins (DEPs) associated with the TG genotype, and 522 proteins associated with ES exposure in TG mice, of which 29 were overlapping. "TG-CTL versus TG-ES" proteins were DEPs from the contrast at 10 months, as there were no DEPS at 4 months.

To visualize the trajectory of differential expression over time, we adopted a Log2FC ratio approach,[13] generating a ΔLog2FC value per protein per contrast (i.e., $\Delta\text{Log2FC} = \text{Log2FC}_{10\text{months}} - \text{Log2FC}_{4\text{months}}$), and ordered proteins based on increasing ΔLog2FC values. While this proxy measure is not able to account for the absolute magnitude or direction of change in each protein across age, it provides an indication of which synaptosomal proteins are more affected by amyloidosis with increasing age (Figure 6B). Using this approach, we find that "WT-CTL versus TG-CTL" proteins (i.e., those impacted because of TG genotype) mostly have negative ΔLog2FC values, although those with positive ones include proteins described to be relevant for AD, for example, Apoe, App, and Clu (Table S9). Notably, the ΔLog2FC values of these three proteins within the TG-CTL versus TG-ES contrast (Figure 6C) take on a qualitatively different pattern. Consistent with this, the ΔLog2FC values of "TG-CTL versus TG-ES" proteins (i.e., those induced when TG mice are ES-exposed) in both contrasts were also largely incongruent. These induced differences in expression were also noticeable for proteins involved in mitochondrial, cytoskeletal, and astrocytic-synaptic processes (Figure 6B-C). While descriptive, these data support the hypotheses that ES exposure leads to a different trajectory in TG mice.

4 | DISCUSSION

We here studied how ES influenced the effects of transgenic Aβ overexpression on the hippocampal synaptosome at early (4 months) and late (10 months) pathological stages. ES-exposed WT mice at 4 months exhibited synaptosomal alterations, involving pathways similar to those induced in control APP/PS1 mice at the same age. Both were characterized by a relative upregulation of mitochondrial proteins and a downregulation of actin-related proteins. These shared alterations at 4 months were also evident at the ultrastructural level, evidenced by the reduced mitochondrial counts in the pre- and post-synapse of APP/PS1 and ES-exposed mice, respectively. These were not associated with ultrastructural changes in synapse size or synaptic vesicles. At 10 months of age, ES exposure had heavily impacted the synaptosomal proteomic profile in APP/PS1, but not WT, mice, including alterations to astrocytic lipid metabolism-related proteins. Finally, ES modulated the trajectory of changes in mitochondrial proteins across ages and pathological stages in synaptosomes from APP/PS1 mice.

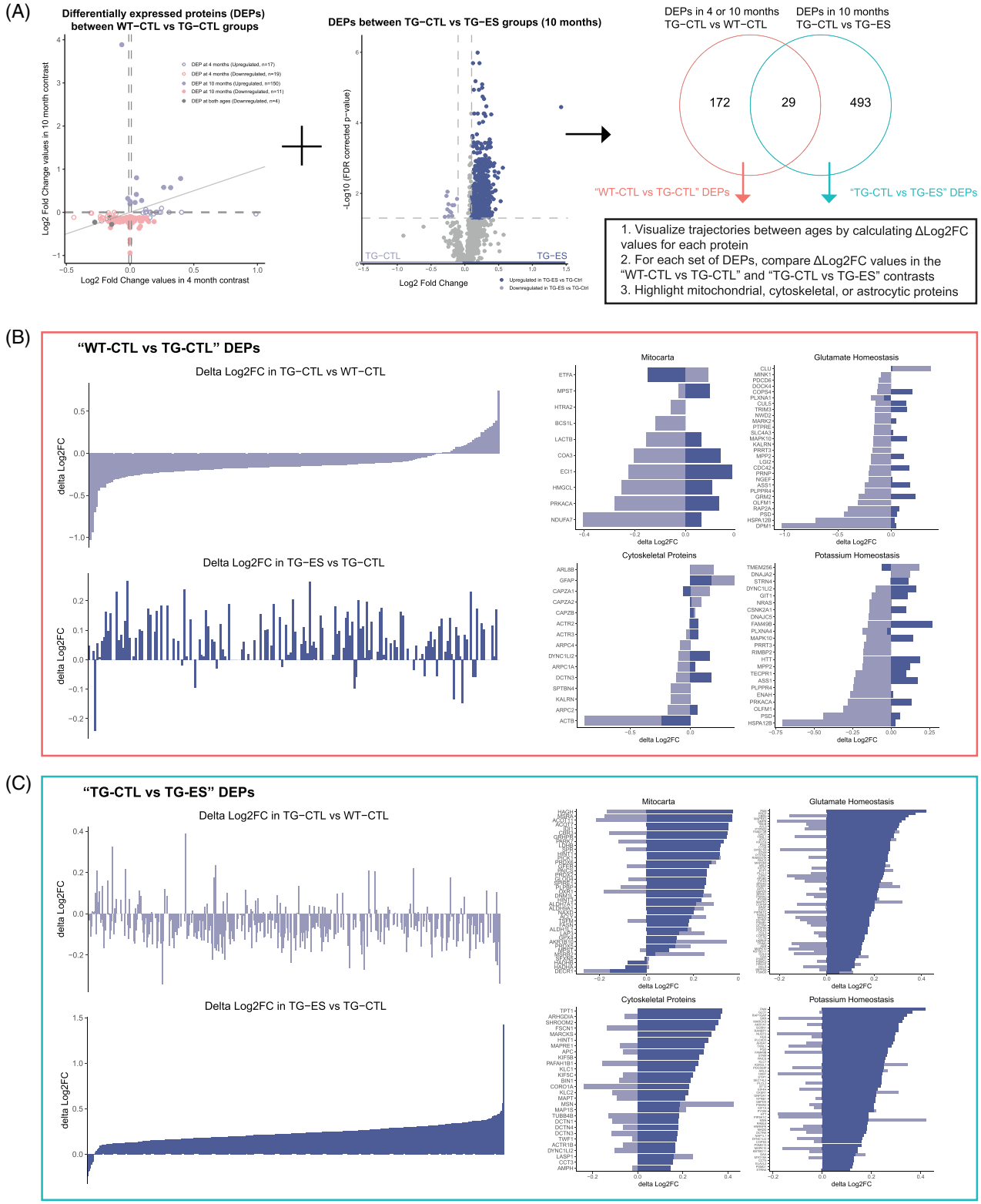

FIGURE 6 Exploring the impact of ES exposure on the temporal pattern of protein changes in synaptosomes from TG mice. (A) Workflow of trajectory analysis. We identified differentially expressed proteins (DEPs, ± Log2FC > 0.1, FDR < 0.05) in synaptosomes from the WT-CTL versus TG-CTL contrasts and TG-CTL versus TG-ES contrasts at 4 and 10 months. A Log2FC ratio between both ages was calculated ($Log2FC_{10months}$ − $Log2FC_{4months}$) to visualize the "standard" progression of each protein in their respective contrasts. We then arranged proteins based on ΔLog2FC values, and highlighted mitochondrial, cytoskeletal, and astrocytic (glutamate and potassium homeostasis) genesets based on literature. (B) Synaptic proteins progressively impacted by amyloidosis ("WT-CTL vs. TG-CTL DEPs") take on a qualitatively distinct trajectory when mice are exposed to ES. (C) "TG-CTL vs. TG-ES DEPs" have progressive changes to synaptic proteins that are mostly absent in the WT-CTL and TG-CTL contrast. Colors of points and bars correspond to experimental group colors depicted in Figures 2A and 4A.

4.1 | Synaptic mitochondria are impacted by both ES exposure and transgenic amyloidosis

Our data support a role for mitochondrial dysfunction in AD pathogenesis,[56] to which ES may contribute. These deficits likely have major implications for synapses, which have high energy demands.[57] Alterations to oxidative phosphorylation and electron transport were previously found in whole hippocampal lysates from 3- and 6-month-old APP/PS1 mice,[58,59] as was a reduction in mitochondrial mass in 6-month-old APP/PS1 mice.[60] Our current data further suggest these alterations occur specifically in the synapses of APP/PS1 mice, accompanied by a decrease in pre-synaptic mitochondria, as also found in the temporal cortex of AD patients.[61] Interestingly, while ultrastructural changes to both synaptic mitochondria and synaptic vesicle have been described in *post mortem* human AD brains,[49] we show here for the first time that synaptic mitochondrial changes are already present at an early disease stage (pre-plaque formation[15]), in APP/PS1 mice, without other ultrastructural synaptic changes. This indicates that mitochondrial changes may precede changes in the number of synaptic vesicles found in more advanced stages of AD.[49,62,63] Notably, the fewer mitochondria found were not larger in area, suggesting this was not a consequence of increased fusion events. The increased mitochondrial protein expression observed in our proteomics data rather suggest a compensation for this mitochondrial loss, although the functional implications of these changes for synaptic energy homeostasis (e.g., ATP production) remain to be determined.

We also found mitochondrial alterations in the synaptosomes of ES-exposed WT mice, in line with impairments to respiration in synaptosomal mitochondria found in adult mice exposed to chronic stress,[64] and our previously reported age-associated ES effects on the hippocampal gene expression of the mitochondrial fission protein Fis1, accompanied by hypothalamic and peripheral disruptions to electron transport chain activity.[65] Intriguingly, our data suggest that mitochondria are a shared substrate via which both ES and Aβ pathology induce hippocampal deficits, disturb energy homeostasis, and potentially altered synaptic physiology. Such convergence would be in line with work demonstrating that early[5] and lifelong[3] stress could induce expression of proteins and pathways related to Aβ proteins in WT rodents, and might explain the lack of additional impact of ES on APP/PS1 mice at 4 months.

Mitochondrial disruption was also prominent in our proteomics data at 10 months, specifically in ES-exposed APP/PS1 mice when compared to control APP/PS1 mice. These effects might be directly related to the increased Aβ plaque load that we previously described in ES-APP/PS1 mice at this age,[16] as amyloid plaque accumulation has been shown to impair mitochondrial structure and function.[66] This aggravation of mitochondrial proteins in ES-exposed APP/PS1 mice might also be caused by alterations in the (re-)activity of the hypothalamic-pituitary-adrenal axis, induced by ES,[67] as stress hormone exposure influences both Aβ metabolism[8,9,68] and mitochondrial health.[69] These interactions might occur during ES exposure, i.e., the first postnatal week, when they might aggravate proteomic alterations present as early as postnatal day 1, as reported in the 5XFAD AD mouse model,[70] or they could emerge at later ages as Aβ pathology accumulates.

These observed mitochondrial alterations could be in part driven by actin cytoskeletal dynamics, which we found to be impacted in both ES and APP/PS1 groups at 4 months. Actin dynamics are crucial for both mitochondrial trafficking[71] and fusion-fission dynamics,[72] as well as implicated in AD, via their aggregation into neuropathological "rods" in AD brains.[73] Supporting the translational relevance of our findings, both energy metabolism and cytoskeletal proteins were dysregulated in synaptoneurosomes[74] and cerebrospinal fluid isolated from AD patients.[75] Moreover, while cytoskeletal disruption did not seem to affect the synapse ultrastructure as investigated in EM, actin-related proteins are also important for receptor trafficking into synapses,[76] and their persistent downregulation in our 10 months CTL-APP/PS1 group (Table S7) might explain the enrichment of SynGO-annotated pathways associated with synaptic vesicle release and recycling in downregulated proteins. While not much is known about actin dysregulation in ES, there is evidence that ES exposure via postnatal social isolation also impairs cytoskeletal dynamics, in turn decreasing synaptic plasticity through deficits in AMPA receptor delivery.[77]

Lastly, the disruptions to mitochondrial and actin-related proteins could also have consequences beyond the neuronal compartments of the synapse, for example, in the motility of peri-synaptic astrocytes (PAP), which undergo cytoskeletal remodeling in response to neuronal activity.[12,27] This might be relevant in the WT-ES group at 4 months as well as APP/PS1 groups (w/wo ES exposure) at 10 months, where we found astrocytic enrichment of differentially expressed proteins. Such potential alterations to PAP motility at the synapse could affect their abilities to regulate extra-synaptic neurotransmitter diffusion,[12] in line with our recent findings that astrocytes in APP/PS1 mice do not show the activity-induced retraction from the synapse as observed in WT animals.[78] This is not expected to be due to an increase in astrocyte number, as supported by our total Vimentin coverage data and our previous work on the GFAP coverage and density.[17]

4.2 | ES effects on the trajectory of age-associated amyloidosis-induced synapse pathology

Despite its impact on the synaptosomal profile in WT mice at 4 months, ES did not strongly alter the proteome of WT mice at 10 months. Correspondingly, while ES had minimal effects on synaptosomes from early pathology (4 months) APP/PS1 mice (despite similar proteins and pathways being dysregulated in both groups), it resulted in large alterations at advanced pathological stage (10 months). Furthermore, APP/PS1 mice exhibited early synaptic changes to amyloid-processing proteins such as App and Ncstn by 4 months, in line with alterations to microgliosis and behavior evident around this age,[15,16] that progressively worsen with age.[13] In ES-exposed APP/PS1 mice, these progressively affected proteins in synaptosomes seemed differentially affected, suggesting that ES exposure alters the trajectory of the APP/PS1 phenotype, in a way that is both age- and pathological-stage-dependent. This is consistent with observations that ES effects

on the synapse (e.g., in adult hippocampal neurogenesis) are more prevalent at younger ages,[26,51] leading to hypotheses that ES affects aging trajectories, and that aged ES-exposed mice still harbor latent ES-associated phenotypes, which could be "unmasked" by additional triggers,[51] exemplified here by the development of amyloidosis.

In line with the age-/pathological-stage-dependent, ES-induced effects described in this study, we had previously reported that ES-exposed APP/PS1 mice display decreases in cell-associated amyloid at 4 months, but an increased Aβ plaque load by 10 months of age.[16] This age-dependent switch in Aβ pathology seems to occur by 6 months, as reflected in the increased expression of amyloidogenic proteins such as BACE1.[18] These age-dependent pathological effects were accompanied by a neuroinflammatory response that were similarly age/pathological-stage-dependent. In particular, while microglial morphology and inflammatory gene expression were lastingly impacted in ES-exposed mice, these effects were more pronounced at postnatal day 9 and 4 months, compared to 10 months.[16] We posited that these age-specific effects would both be driven by, as well as contribute to, the differential pathology load at different ages, and that the astrocytic profile across the lifetime of ES-exposed APP/PS1 mice, while not different in gene expression and morphology, might exhibit alterations in other functional domains due to the increase in amyloid load.[17]

The involvement of astrocytes in our proteomics data is suggested by both the enrichment of astrocytic proteins as well as proteins involved in (mitochondrial) energy metabolism, which astrocytes have a prominent role in.[53] In particular, we found differential expression of two astrocytic proteins: a decrease in Hadha, key in the beta-oxidation of fatty acids,[53] and an increase in Fasn, involved in de novo synthesis of fatty acids.[52] Notably, hippocampal Fasn mRNA expression is also increased in WT-ES mice.[17] These dysregulations, confirmed by immunofluorescence to specifically occur in astrocytes, suggest a role for altered astrocytic lipid synthesis in ES-exposed APP/PS1 mice, which could contribute to increased oxidative stress, a neuroinflammatory and neurodegenerative astrocytic lipid profile[79] and, thus, neurotoxicity.[80] Alterations to astrocytic lipid metabolism in AD patients have recently also been described in a single nucleus RNA sequencing study,[81] and, while we cannot conclude cell type specific effects from our analyses, the changes to astrocytic lipid proteins and synaptic mitochondria, along with an overrepresentation of astrocytic and ROS metabolism annotations in differentially expressed proteins, suggests further dysregulation of lipid metabolism in ES-exposed APP/PS1 mice. Crucially, ES exposure results in age-dependent consequences on lipidomic profiles in the brains of WT mice,[82,83] which can be rescued via dietary intervention.[82] The interactions between these altered synaptosomal and lipidomic profiles, and their functional consequences in the context of synaptic and astrocytic function, remains to be determined.

In conclusion, we show that ES exposure in WT mice results in a similar synaptosomal profile as early Aβ pathology does. At 10 months of age, ES exposure altered the proteomic profile only in synaptosomes from APP/PS1 mice, aggravating alterations induced by advanced Aβ pathology. Mitochondrial dysfunction was implicated at both ages, possibly involving both impaired energy metabolism in the pre- and post-synapse, as well as shifts in lipid metabolism in the astrocytic components. The age-dependent convergence in the synaptic signature induced by both ES and amyloidosis intriguingly gives novel insights as to how early, environmental factors can drive and shape the progression of AD and AD-related pathologies.

AUTHOR CONTRIBUTIONS

Study conceptualization: Aniko Korosi, Mark H. G. Verheijen, Janssen M. Kotah, Mandy S. J. Kater. Animal work and tissue collection: Janssen M. Kotah, Mandy S. J. Kater, Niek Brosens, Sylvie L. Lesuis. Downstream analysis of mass spectrometry data: Janssen M. Kotah, Mandy S. J. Kater, Frank T. W. Koopmans. EM sample preparation and imaging: Mandy S. J. Kater, Thomas M. Blok. EM analysis: Mandy S. J. Kater, Thomas M. Blok, and Roberta Tandari. Validation staining, imaging, analysis: Luca Marchetto, Ella Yusaf. Figures and tables: Janssen M. Kotah. Manuscript drafting and writing: Janssen M. Kotah, Aniko Korosi. Manuscript review and editing: Janssen M. Kotah, Mandy S. J. Kater, Sylvie L. Lesuis, Paul J. Lucassen, Frank T. W. Koopmans, August B. Smit, Harm J. Krugers, Aniko Korosi, Mark H. G. Verheijen. All co-authors have read the final version of the manuscript, and consent to its submission for publication.

ACKNOWLEDGMENTS

The authors thank Aline Mak for assistance with EM sample preparation, Miguel Gonzalez-Lozano and Jan van Weering for help with EM analysis, Yvonne Gouwenberg for synaptosome isolations and Iryna Paliukhovich and Remco Klaassen for technical assistance with MS sample preparation and MS data analysis. P.J.L., M.S.J.K., M.H.G.V., H.K., A.B.S., and A.K. are supported by Alzheimer Nederland and by the ZonMW Memorabel MODEM program, T.M.B. by an ENW-M1 grant of the Dutch Research Council (NWO), and PJL by the Center for Urban Mental Health, UvA.

CONFLICT OF INTEREST STATEMENT

The authors declare no conflicts of interest. Author disclosures are available in the supporting information.

CONSENT STATEMENT

N/A; This study did not involve any human participants.

SUPPLEMENTARY INFORMATION AND DATA AVAILABILITY

Our proteomics data are publicly available and can be accessed online using a web app, via https://amsterdamstudygroup.shinyapps.io/ES_Synaptosome_Proteomics_Visualizer/. Tables containing gene lists and results of (downstream) proteomics analyses are included as supplementary files. All other data will be made available upon request.

ORCID

Aniko Korosi https://orcid.org/0000-0001-9701-3331

REFERENCES

1. Karch CM, Goate AM. Alzheimer's disease risk genes and mechanisms of disease pathogenesis. *Biol Psychiatry*. 2015;77(1):43-51.
2. Andrews SJ, Fulton-Howard B, Goate A. Interpretation of risk loci from genome-wide association studies of Alzheimer's disease. *Lancet Neurol*. 2020;19(4):326-335.
3. Lyons CE, Zhou X, Razzoli M, et al. Lifelong chronic psychosocial stress induces a proteomic signature of Alzheimer's disease in wildtype mice. *Eur J Neurosci*. 2022;55(9-10):2971-2985.
4. Martisova E, Solas M, Gerenu G, Milagro FI, Campion J, Ramirez MJ. Mechanisms involved in BACE upregulation associated to stress. *Curr Alzheimer Res*. 2012;9(7):822-829.
5. Martisova E, Aisa B, Guerenu G, Javier Ramirez M. Effects of early maternal separation on biobehavioral and neuropathological markers of Alzheimer's disease in adult male rats. *Curr Alzheimer Res*. 2013;10(4):420-432.
6. Donley GAR, Lönnroos E, Tuomainen TP, Kauhanen J. Association of childhood stress with late-life dementia and Alzheimer's disease: the KIHD study. *Eur J Public Health*. 2018. Published online.
7. Wang L, Yang L, Yu L, et al. Childhood physical neglect promotes development of mild cognitive impairment in old age—A case-control study. *Psychiatry Res*. 2016;242(C):13-18.
8. Hoeijmakers L, Lesuis SL, Krugers H, Lucassen PJ, Korosi A. A preclinical perspective on the enhanced vulnerability to Alzheimer's disease after early-life stress. *Neurobiol Stress*. 2018;8:172-185.
9. Lesuis SL, Hoeijmakers L, Korosi A, et al. Vulnerability and resilience to Alzheimer's disease: early life conditions modulate neuropathology and determine cognitive reserve. *Alzheimer's Res Ther*. 2018;10(1):1-20.
10. Jankowsky JL, Slunt HH, Ratovitski T, Jenkins NA, Copeland NG, Borchelt DR. Co-expression of multiple transgenes in mouse CNS: a comparison of strategies. *Biomol Eng*. 2001;17(6):157-165.
11. Jankowsky JL, Fadale DJ, Anderson J, et al. Mutant presenilins specifically elevate the levels of the 42 residue β-amyloid peptide in vivo: evidence for augmentation of a 42-specific γ secretase. *Hum Mol Genet*. 2004;13(2):159-170.
12. Badia-Soteras A, Heistek TS, Kater MSJ, et al. Retraction of astrocyte leaflets from the synapse enhances fear memory. *Biol Psychiatry*. October 2022. Published online.
13. van der Spek SJF, Gonzalez-Lozano MA, Koopmans F, et al. Age-dependent hippocampal proteomics in the app/ps1 alzheimer mouse model: a comparative analysis with classical swath/dia and directdia approaches. *Cells*. 2021;10(7).
14. López-González I, Schlüter A, Aso E, et al. Neuroinflammatory signals in alzheimer disease and APP/PS1 transgenic mice: correlations with plaques, tangles, and oligomeric species. *J Neuropathol Exp Neurol*. 2015;74(4):319-344.
15. Kater MSJ, Huffels CFM, Oshima T, et al. Prevention of microgliosis halts early memory loss in a mouse model of Alzheimer's disease. *Brain Behav Immun*. 2022;18. Published online October.
16. Hoeijmakers L, Ruigrok SR, Amelianchik A, et al. Early-life stress lastingly alters the neuroinflammatory response to amyloid pathology in an Alzheimer's disease mouse model. *Brain Behav Immun*. 2017;63:160-175.
17. Abbink MR, Kotah JM, Hoeijmakers L, et al. Characterization of astrocytes throughout life in wildtype and APP/PS1 mice after early-life stress exposure. *J Neuroinflammation*. 2020;17(1):91.
18. Lesuis SL, Weggen S, Baches S, Lucassen PJ, Krugers HJ. Targeting glucocorticoid receptors prevents the effects of early life stress on amyloid pathology and cognitive performance in APP/PS1 mice. *Transl Psychiatry*. 2018;8(1):53.
19. Lesuis SL, Lucassen PJ, Krugers HJ. Early life stress amplifies fear responses and hippocampal synaptic potentiation in the APPswe/PS1dE9 Alzheimer mouse model. *Neuroscience*. 2021;454:151-161.
20. Lesuis SL, Lucassen PJ, Krugers HJ. Early life stress impairs fear memory and synaptic plasticity; a potential role for GluN2B. *Neuropharmacology*. 2019;149:195-203.
21. Lesuis SL, Kaplick PM, Lucassen PJ, Krugers HJ. Treatment with the glutamate modulator riluzole prevents early life stress-induced cognitive deficits and impairments in synaptic plasticity in APPswe/PS1dE9 mice. *Neuropharmacology*. 2019:1-9. Published online.
22. Davies CA, Mann DMA, Sumpter PQ, Yates PO. A quantitative morphometric analysis of the neuronal and synaptic content of the frontal and temporal cortex in patients with Alzheimer's disease. *J Neurol Sci*. 1987;78(2):151-164.
23. Scheff SW, Price DA, Schmitt FA, Dekosky ST, Mufson EJ. Synaptic alterations in CA1 in mild Alzheimer disease and mild cognitive impairment. *Neurology*. 2007;68(18):1501-1508.
24. Arendt T. Synaptic degeneration in Alzheimer's disease. *Acta Neuropathol*. 2009;118(1):167-179.
25. Kothapalli SVVN, Benzinger TL, Aschenbrenner AJ, et al. Quantitative gradient echo MRI identifies dark matter as a new imaging biomarker of neurodegeneration that precedes tisssue atrophy in early Alzheimer's disease. *J Alzheimer's Dis*. 2022;85(2):901-920.
26. Hoeijmakers L, Amelianchik A, Verhaag F, Kotah J, Lucassen PJ, Korosi A. Early-life stress does not aggravate spatial memory or the process of hippocampal neurogenesis in adult and middle-aged APP/PS1 mice. *Front Aging Neurosci*. 2018;10(MAR).
27. Sapkota D, Kater MSJ, Sakers K, et al. Activity-dependent translation dynamically alters the proteome of the perisynaptic astrocyte process. *Cell Rep*. 2022;41(3):111474.
28. Koopmans F, Ho JTC, Smit AB, Li KW. Comparative analyses of data independent acquisition mass spectrometric approaches: dIA, WiSIM-DIA, and Untargeted DIA. *Proteomics*. 2018;18(1).
29. Goeminne LJE, Gevaert K, Clement L. Peptide-level robust ridge regression improves estimation, sensitivity, and specificity in data-dependent quantitative label-free shotgun proteomics. *Mol Cell Proteomics*. 2016;15(2):657-668.
30. Gao CH, Yu G, Cai P. ggVennDiagram: an intuitive, easy-to-use, and highly customizable R package to generate venn diagram. *Front Genet*. 2021;12:1598.
31. Skene NG, Grant SGN. Identification of vulnerable cell types in major brain disorders using single cell transcriptomes and expression weighted cell type enrichment. *Front Neurosci*. 2016;10(JAN):16.
32. Zeisel A, M̈oz-Manchado AB, Codeluppi S, et al. Cell types in the mouse cortex and hippocampus revealed by single-cell RNA-seq. *Science (80-)*. 2015;347(6226):1138-1142.
33. Raudvere U, Kolberg L, Kuzmin I, et al. G:profiler: a web server for functional enrichment analysis and conversions of gene lists (2019 update). *Nucleic Acids Res*. 2019;47(W1):W191-W198.
34. Koopmans F, van Nierop P, Andres-Alonso M, et al. SynGO: an evidence-based, expert-curated knowledge base for the synapse. *Neuron*. 2019;103(2):217-234.
35. Sayols S, rrvgo: a Bioconductor package to reduce and visualize Gene Ontology terms. Published online 2020.
36. Rath S, Sharma R, Gupta R, et al. MitoCarta3.0: an updated mitochondrial proteome now with sub-organelle localization and pathway annotations. *Nucleic Acids Res*. 2021;49(D1):D1541-D1547.
37. Tea RStudio, m. RStudio: Integrated Development for R. Published online 2020.
38. Carbon S, Ireland A, Mungall CJ, et al. AmiGO: online access to ontology and annotation data. *Bioinformatics*. 2009;25(2):288-289.
39. Soto JS, Jami-Alahmadi Y, Chacon J, et al. Astrocyte-neuron subproteomes and obsessive-compulsive disorder mechanisms. *Nature*. 2023;616(7958):764-773.
40. Machesky LM, Mullins RD, Higgs HN, et al. Scar, a WASp-related protein, activates nucleation of actin filaments by the Arp2/3 complex. *Proc Natl Acad Sci U S A*. 1999;96(7):3739-3744.

41. Cholet N, Pellerin L, Magistretti PJ, Hamel E. Similar perisynaptic glial localization for the Na+,K+-ATPase alpha 2 subunit and the glutamate transporters GLAST and GLT-1 in the rat somatosensory cortex. *Cereb cortex*. 2002;12(5):515-525.
42. Minelli A, DeBiasi S, Brecha NC, Zuccarello LV, Conti F. GAT-3, a high-affinity GABA plasma membrane transporter, is localized to astrocytic processes, and it is not confined to the vicinity of GABAergic synapses in the cerebral cortex. *J Neurosci*. 1996;16(19):6255-6264.
43. Uhlén M, Fagerberg L, Hallström BM, et al. Proteomics. Tissue-based map of the human proteome. *Science*. 2015;347(6220).
44. Mick DU, Vukotic M, Piechura H, et al. Coa3 and Cox14 are essential for negative feedback regulation of COX1 translation in mitochondria. *J Cell Biol*. 2010;191(1):141.
45. Ruan Y, Hu J, Che Y, et al. CHCHD2 and CHCHD10 regulate mitochondrial dynamics and integrated stress response. *Cell Death Dis*. 2022;13(2).
46. Hsu F, Spannl S, Ferguson C, Hyman AA, Parton RG, Zerial M. Rab5 and Alsin regulate stress-activated cytoprotective signaling on mitochondria. *Elife*. 2018;7.
47. Zhang G, Li X, Sun Y, Wang X, Liu G, Huang Y. A genetic screen identifies Etl4-deficiency capable of stabilizing the haploidy in embryonic stem cells. *Stem Cell Reports*. 2021;16(1):29-38.
48. Romero MF, Chen AP, Parker MD, Boron WF. The SLC4 family of bicarbonate (HCO3-) Transporters. *Mol Aspects Med*. 2013;34(2-3):159.
49. Wang W, Zhao F, Lu Y, et al. Damaged mitochondria coincide with presynaptic vesicle loss and abnormalities in alzheimer's disease brain. *Acta Neuropathol Commun*. 2023;11(1):1-15.
50. Heneka MT, Carson MJ, Khoury J El, et al. Neuroinflammation in Alzheimer's disease. *Lancet Neurol*. 2015;14(4):388-405.
51. Kotah JM, Hoeijmakers L, Nutma E, Lucassen PJ, Korosi A. Early-life stress does not alter spatial memory performance, hippocampal neurogenesis, neuroinflammation, or telomere length in 20-month-old male mice. *Neurobiol Stress*. 2021;15:100379.
52. van Deijk ALLF, Camargo N, Timmerman J, et al. Astrocyte lipid metabolism is critical for synapse development and function in vivo. *Glia*. 2017;65(4):670-682.
53. Rose J, Brian C, Pappa A, Panayiotidis MI, Franco R. Mitochondrial metabolism in astrocytes regulates brain bioenergetics, neurotransmission and redox balance. *Front Neurosci*. 2020;14:1155.
54. Karpf J, Unichenko P, Chalmers N, et al. Dentate gyrus astrocytes exhibit layer-specific molecular, morphological and physiological features. *Nat Neurosci*. 2022;25(12):1626-1638.
55. Batiuk MY, Martirosyan A, Wahis J, et al. Identification of region-specific astrocyte subtypes at single cell resolution. *Nat Commun*. 2020;11(1):1220.
56. Ashleigh T, Swerdlow RH, Beal MF. The role of mitochondrial dysfunction in Alzheimer's disease pathogenesis. *Alzheimers Dement*. 2023;19(1):333-342.
57. Faria-Pereira A, Morais VA. Synapses: the Brain's energy-demanding sites. *Int J Mol Sci*. 2022;23(7):3627.
58. Clement A, Madsen MJ, Kastaniegaard K, Wiborg O, Asuni AA, Stensballe A. Chronic stress induces hippocampal mitochondrial damage in APPPS1 model mice and wildtype littermates. *J Alzheimer's Dis*. 2022;87(1):1-14.
59. He K, Nie L, Zhou Q, et al. Proteomic profiles of the early mitochondrial changes in APP/PS1 and ApoE4 transgenic mice models of Alzheimer's disease. *J Proteome Res*. 2019;18(6):2632-2642.
60. Bartolome F, De La Cueva M, Pascual C, et al. Amyloid β-induced impairments on mitochondrial dynamics, hippocampal neurogenesis, and memory are restored by phosphodiesterase 7 inhibition. *Alzheimer's Res Ther*. 2018;10(1):1-15.
61. Pickett EK, Rose J, McCrory C, et al. Region-specific depletion of synaptic mitochondria in the brains of patients with Alzheimer's disease. *Acta Neuropathol*. 2018;136(5):747-757.
62. Andersen JV, Skotte NH, Christensen SK, et al. Hippocampal disruptions of synaptic and astrocyte metabolism are primary events of early amyloid pathology in the 5xFAD mouse model of Alzheimer's disease. *Cell Death Dis 2021 1211*. 2021;12(11):1-13.
63. Chakroborty S, Hill ES, Christian DT, et al. Reduced presynaptic vesicle stores mediate cellular and network plasticity defects in an early-stage mouse model of Alzheimer's disease. *Mol Neurodegener*. 2019;14(1):1-21.
64. Shaw GA, Hyer MM, Targett I, et al. Traumatic stress history interacts with sex and chronic peripheral inflammation to alter mitochondrial function of synaptosomes. *Brain Behav Immun*. 2020;88:203-219.
65. Ruigrok SR, Yim K, Emmerzaal TL, et al. Effects of early-life stress on peripheral and central mitochondria in male mice across ages. *Psychoneuroendocrinology*. 2021:132.
66. Xie H, Guan JS, Borrelli LA, Xu J, Serrano-Pozo A, Bacskai BJ. Mitochondrial alterations near amyloid plaques in an Alzheimer's disease mouse model. *J Neurosci*. 2013;33(43):17042-17051.
67. van Bodegom M, Homberg JR, Henckens MJAG. Modulation of the hypothalamic-pituitary-adrenal axis by early life stress exposure. *Front Cell Neurosci*. 2017;11(Pt 3):1222-1233.
68. Sotiropoulos I, Silva JM, Gomes P, Sousa N, Almeida OFX. Stress and the etiopathogenesis of Alzheimer's disease and depression. *Adv Exp Med Biol*. 2019;1184:241-257.
69. Liu W, Zhou C. Corticosterone reduces brain mitochondrial function and expression of mitofusin, BDNF in depression-like rodents regardless of exercise preconditioning. *Psychoneuroendocrinology*. 2012;37(7):1057-1070.
70. Uras I, Karayel-Basar M, Sahin B, Baykal AT. Detection of early proteomic alterations in 5xFAD Alzheimer's disease neonatal mouse model via MALDI-MSI. *Alzheimer's Dement*. 2023. Published online.
71. Aiken J, Holzbaur ELF. Cytoskeletal regulation guides neuronal trafficking to effectively supply the synapse. *Curr Biol*. 2021;31(10):R633-R650.
72. Moore AS, Wong YC, Simpson CL, Holzbaur ELF. Dynamic actin cycling through mitochondrial subpopulations locally regulates the fission-fusion balance within mitochondrial networks. *Nat Commun*. 2016;7:12886.
73. Bamburg JR, Bernstein BW. Actin dynamics and cofilin-actin rods in alzheimer disease. *Cytoskeleton*. 2016;73(9):477-497.
74. Hesse R, Hurtado ML, Jackson RJ, et al. Comparative profiling of the synaptic proteome from Alzheimer's disease patients with focus on the APOE genotype. *Acta Neuropathol Commun*. 2019;7(1):1-18.
75. del Campo M, Peeters CFW, Johnson ECB, et al. CSF proteome profiling across the Alzheimer's disease spectrum reflects the multifactorial nature of the disease and identifies specific biomarker panels. *Nat Aging 2022 211*. 2022;2(11):1040-1053.
76. Gu J, Lee CW, Fan Y, et al. ADF/cofilin-mediated actin dynamics regulate AMPA receptor trafficking during synaptic plasticity. *Nat Neurosci*. 2010;13(10):1208-1215.
77. Tada H, Miyazaki T, Takemoto K, et al. Social isolation suppresses actin dynamics and synaptic plasticity through ADF/cofilin inactivation in the developing rat barrel cortex. *Sci Rep*. 2017;7(1):8471.
78. Kater MSJ, Badia-Soteras A, van Weering JRT, Smit AB, Verheijen MHG. Electron microscopy analysis of astrocyte-synapse interactions shows altered dynamics in an Alzheimer's disease mouse model. *Front Cell Neurosci*. 2023;17:1085690.
79. Mi Y, Qi G, Vitali F, et al. Loss of fatty acid degradation by astrocytic mitochondria triggers neuroinflammation and neurodegeneration. *Nat Metab 2023 53*. 2023;5(3):445-465.
80. Guttenplan KA, Weigel MK, Prakash P, et al. Neurotoxic reactive astrocytes induce cell death via saturated lipids. *Nature*. 2021;599(7883):102-107.
81. Mathys H, Peng Z, Boix CA, et al. Single-cell atlas reveals correlates of high cognitive function, dementia, and resilience to Alzheimer's disease pathology. *Cell*. 2023;186(20):4365-4385.
82. Yam KY, Schipper L, Reemst K, et al. Increasing availability of ω-3 fatty acid in the early-life diet prevents the early-life stress-induced

cognitive impairments without affecting metabolic alterations. *FASEB J*. 2019;33(4):5729-5740.

83. Reemst K, Broos JY, Abbink MR, et al. Early-life stress and dietary fatty acids impact the brain lipid/oxylipin profile into adulthood, basally and in response to LPS. *Front Immunol*. 2022;13:967437.

SUPPORTING INFORMATION

Additional supporting information can be found online in the Supporting Information section at the end of this article.

How to cite this article: Kotah JM, Kater MSJ, Brosens N, et al. Early-life stress and amyloidosis in mice share pathogenic pathways involving synaptic mitochondria and lipid metabolism. *Alzheimer's Dement*. 2024;20:1637–1655. https://doi.org/10.1002/alz.13569